Jihočeská univerzita v Českých Budějovicích

Přírodovědecká fakulta

Role makrofágů v mobilizaci lipidových zásob v průběhu metamorfózy a post-metamorfickém vývoji u *Drosophila melanogaster*

Rigorózní práce

Mgr. Adéla Danielová

České Budějovice 2025

Citování této práce: Danielová, A. (2025): Role makrofágů v mobilizaci lipidových zásob v průběhu metamorfózy a post-metamorfickém vývoji u *Drosophila melanogaster*. RNDr. Thesis, in Czech – 26 pp. Přírodovědecká fakulta, Jihočeská univerzita, České Budějovice, Česká republika.

Anotace:
V průběhu metamorfózy holometabolního hmyzu dochází ke kompletní přestavbě těla jedince, což je značně energeticky náročný proces. Využití energeticky bohatých látek je totiž klíčový pro proces vykuklení a následný post-metamorfický vývoj, avšak dosud nebylo popsáno, jak dochází k přetrasformování nutričně bohatých látek z larválního stadia do těla dospělce. Tato práce ukazuje, že v průběhu metamorfózy *Drosophila melanogaster* dochází k infiltraci larválního tukového tělesa makrofágy, které přijímají adipocytární fenotyp a přetvářejí umírající buňky larválního tukového tělesa do lipoproteinů a zásobních peptidů. Tyto nutričně bohaté látky jsou zásadní pro včasný vývoj ovárií a plodnost dospělých samic.

Annotation:
Holometabolous insect must undergo a major transformation of their body plan during metamorphosis, which is a highly energy-demanding process. The utilization of energy-rich substances is crutial for the process of eclosion and subsequent post-metamorphic development. However, it has not yet been described how the transformation of nutrient-rich substances from the larval stage into teh adult body occurs. This study demostrates that during the metamorphosis of *Drosophila* melanogaster, larval fat body is infiltrated by macrophages, which adopt an adipocyte-like phenotype and convert dying cells of the latval fat body into lipoproteins and storage peptides. These nutrient-rich substances are essential for the early development of ovaries and the fecundity of adult females.

Prohlášení

Prohlašuji, že jsem autorem této kvalifikační práce a že jsem ji vypracoval(a) pouze s použitím pramenů a literatury uvedených v seznamu použitých zdrojů.

Praha 28. 4. 2025 Mgr. Adéla Danielová

Autorské příspěvky:

Níže uvedený spoluautor plně uznává, že Adéla Danielová je druhým autorem zde prezentované publikace, která obsahuje výsledky její bakalářské a diplomové práce. Adéla samostatně provedla experimenty zkoumající počet a morfologii adipocytů v několika časových bodech průběhu metamorfózy a raného post-metamorfického vývoje jedince (velikost a počet adipocytů, velikost a počet RNA-proteinových granulí a lipidových kapek). Pro tyto účely připravila parafinové řezy obarvené Malloryho trichrom barvením nebo toluidinovou modří a také vykřížila muší linii s fluorescenčně značenými adipocyty a makrofágy. Adéla zkoumala také expresi genů zapojených v sekreci lipoproteinů a metabolismus ceramidů v larválním tukovém tělese během metamorfózy a raného post-metamorfického vývoje. Podílela se jak na analýze snímků z elektronového mikroskopu, tak na přípravě rukopisu. Spoluautor tyto skutečnosti potvrzuje svým podpisem.

Mgr. Adam Bajgar, Ph.D

1. Úvod

1.1 Obecný přehled

Vývoj holometabolního hmyzu je rozdělen na tři odlišná stádia, která jsou specifická svými nároky na podmínky a potřeby nutné k dokončení životního cyklu. Tato stádia jsou ekologicky oddělená a zahrnují období růstu a akumulace živin potřebných pro metamorfózu a následující post-metamorfický vývoj a na období reprodukční aktivity (Vilmos, 1998). Proces metamorfózy je charakteristický významnou přestavbou těla holometabolního hmyzu.

Během metamorfózy podstupuje velká část larválních tkání histolýzu a většina dospělých tkání a orgánů se vyvíjí z imaginálních disků (ten Brink, de Roos and Dieckmann, 2019). Jednou z tkání podstupující histolýzu je také larvální tukové těleso, které je zodpovědné za akumulaci a následný výdej dostatečného množství esenciálních nutričně-bohatých látek. Takto jsou zásobní živiny nashromážděné během larválního stadia přetransformovány do životní fáze dospělce, kde sehrávají klíčovou roli v post-metamorfickém vývoji (Aguila *et al.*, 2007; Storelli *et al.*, 2019). Avšak přesný mechanismus, kterým je umožněna mobilizace nutričních zásob z tukového tělesa během metamorfózy nebyl dosud plně objasněn.

Vývoj hmyzu je řízen steroidním hormonem ekdysonem, který je významným hráčem v iniciaci autofagie larválních tkání včetně larválního tukového tělesa. V přítomnosti ekdysonu dochází k jeho navázání na ekdysonový receptor (EcR), což vede ke ztrátě integrinů v plazmatické membráně zodpovědných za odblokování procesu autofagie (D'Avino and Thummel, 2000). Kromě toho hraje ekdyson roli v aktivaci makrofágů během metamorfózy, což se projevuje jejich zvýšenou mobilitou, expresí enzymů nutných k metabolismu mimobuněčné hmoty a enzymatických kaskád zapojených v procesu zvaném efferocytóza (Regan *et al.*, 2013).

V tukovém tělese jsou primárně ukládány energeticky bohaté látky jako karbohydráty, lipidy a peptidy, čímž tukové těleso plní funkci centrálního metabolického orgánu hmyzu, ze kterého se v případě potřeby transportují nutrienty do hemolymfy a následně i metabolicky aktivních tkání (Pocas, Crosbie and Mirth, 2022). Při nástupu metamorfózy jsou zásobní peptidy z hemolymfy resorbovány do cytosolu adipocytů tukového tělesa a společně s autofagií drsného endoplazmatického retikula a mitochondrií vytvářejí ribonukleoproteinové granule (RNP-granules), což naznačuje, že v tuto dobu již

pravděpodobně dochází k útlumu translace (Locke and Collins, 1965; Tysell and Butterworth, 1978; Butterworth, Emerson and Rasch, 1988; Bond *et al.*, 2011). Hromaděním peptidů a karbohydrátů uvnitř larválních adipocytů dochází k rozvoji jejich hypertrofie, která má za následek infiltraci makrofágů této tkáně (Nelliot, Bond and Hoshizaki, 2006). Infiltrace tukové tkáně makrofágy byla popsána především u obézních savců, ale také během akutního hladovění nebo v důsledku infekce, proto je velmi zajímavé studovat úlohu makrofágů v obdobném procesu i u drosophily, kde se zjevně jedná o nepatologický vývojově kontrolovaný proces.

1.2 Role larválního tukového tělesa u *Drosophila melanogaster*

Tukové těleso hmyzu hraje roli centrálního metabolického orgánu a společně s hemolymfou představují hlavní rezervoár glykoproteinů, lipidů a peptidů těla hmyzu (Nelliot, Bond and Hoshizaki, 2006). Larvální tukové těleso je tvořeno jednou vrstvou dlaždicovitých buněk, které jsou k sobě těsně přimknuty a obaleny bazální laminou (Dai *et al.*, 2017).

Cytosol larválních adipocytů je z převážné většiny vyplněn lipidovými kapkami, které jsou tvořeny především triglyceridy. Tukové těleso je zodpovědné za produkci transportních lipoproteinů označovaných jako lipophoriny, které jsou zapojené v mobilizaci lipidů během metamorfózy (Kambysellis, 1977). Lipophoriny jsou syntetizovány v neaktivní formě (Apolipophorin I/II) a k jejich aktivaci a transportu je nutná přítomnost lipidového transportního proteinu (Ltp) (Palm *et al.*, 2012). Ze střeva jsou lipidy transportovány nejčastěji v podobě triglycerolů (TAG), diacylglycerolů (DAG) a cholesteryl-esterů do hemolymfy odkud se dostávají do tukového tělesa, kde se ukládají v podobě TAG nebo jsou spotřebovány jako zdroj energie (Jouni, Zamora and Wells, 2002). Transport lipidů je závislý na přítomnosti mikrosomálního triglyceridového transportního proteinu (Mtp), který je zodpovědný za vazbu lipidů k proteinu Ltp (Palm *et al.*, 2012).

Vedle své metabolické funkce hraje tukové těleso klíčovou roli v sekreci esenciálních hormonů zodpovědných za regulaci vývoje hmyzu, zprostředkování imunitní odpovědi produkcí antimikrobiálních peptidů a syntéze hormonů zodpovědných za řízení metamorfózy a lipolýzy (Tapadia and Verma, 2012; Azeez, Meintjes and Chamunorwa, 2014).

Na konci posledního larválního instaru se v adipocytech začínají tvořit elektron-densitní struktury, které vznikají resorpcí zásobních peptidů z hemolymfy a autofagií

některých organel adipocytů (Rode *et al.*, 2018). Za použití elektronové mikroskopie bylo ukázáno, že tyto útvary obsahují autofagosomy s částečně degradovanými mitochondriemi a endoplazmatickým retikulem.

Pod vlivem steroidního hormonu ekdysonu, produkovaného z prothorakální žlázy, se na počátku období kukly larvální tukové těleso rozpadá na jednotlivé adipocyty, které se zvětšují a mění svůj tvar z polygonálních na sférický (Dai *et al.*, 2017). Nemění se však pouze jejich morfologie, ale také ultrastruktura, neboť ve stadiu kukly a během prvních 72 hodin po vykuklení lipidové kapky a RNP granule larválních adipocytů mění svou velikost a počet (Danielová, 2021).

Během metamorfózy lipidy uložené v lipidových kapkách slouží jako hlavní zdroj energie, protože v tomto období moucha nepřijímá potravu a jsou na ni tak kladeny vysoké energetické nároky. Zároveň jsou lipidy využívány během post-metamorfického vývoje, kdy hrají nezastupitelnou roli v maturaci reprodukčních orgánů, formování dospělého tukového tělesa a zrání kutikuly (Aguila *et al.*, 2007; Storelli *et al.*, 2019). Množství nutrientů uložených v larválním tukovém tělese se tak stává klíčové pro plodnost dospělců (Briegel, 1990). Lipidy uložené v larválním tukovém tělese jsou zcela spotřebovány během prvních tří dnů života dospělce (Rehman and Varghese, 2021).

1.3 Makrofágy larvální tukové tkáně u *Drosophila melanogaster*

Makrofágy hrají klíčovou roli v likvidaci umírajících, poškozených a senescentních buněk, které odstraňují procesem označovaným jako efferocytóza, která se tak stává esenciální pro udržení homeostáze (Regan *et al.*, 2013). Regan a kol. ukazují, že během metamorfózy se v cytosolu makrofágů vyskytují velké vakuoly, které obsahují efferocytované sarkolyty pocházející z larválních svalů (Ghosh, Ghosh and Mandal, 2020; Regan *et al.*, 2013). Dále bylo dokumentováno, že mobilita makrofágů a tedy přítomnost těchto vakuol je během metamorfózy indukována ekdysonem. Makrofágy s geneticky indukovanou overexpresí dominantně negativní formy ekdysonového receptoru tyto vakuoly postrádaly, což naznačuje, že ekdyson je nezbytný pro jejich aktivaci a efferocytózu senescentních buněk (Regan *et al.*, 2013).

V důsledku nashromáždění nadbytečného množství lipidů prostřednictvím efferocytózy vznikají v makrofázích multilamelární tělíska jako odpověď na zvýšenou lysozomální aktivitu a hromadění lipidů v buňce (Schmitz and Muller, 1991).

Makrofágy nesou ve své buněčné membráně Croquemort, což je scavenger receptor

zodpovědný nejen za rozpoznání patogenů a apoptotických buněk, ale také za zachytávání unikající lipidů z adipocytů (Franc *et al.*, 1996). Bylo ukázáno, že během metamorfózy z larválních adipocytů unikají lipidové kapky, které jsou zachytávány makrofágy, ve kterých pak vytvářejí intracellulární vesikuly (Ghosh, Ghosh and Mandal, 2020). Obsah těchto vesikulů je později enzymaticky štěpen v lysosomech.

V reakci na zachytávání lipidů makrofágy mění svou fenotypovou polarizaci a stávají se z nich makrofágy označované jako „foamy“, tedy makrofágy takzvaně zpěněné (Haka *et al.*, 2016). Tento stav je typický pro savčí makrofágy tvořící „crown-like“ (prstencovité) struktury okolo adipocytů v obézní tukové tkáni (Cinti *et al.*, 2005).

Přítomnost makrofágů v histolyzujícím tukovém tělese drosophily byla již několikrát dokumentována. Výzkum laboratoře vedené doktorkou Mandal ukázal, že během metamorfózy makrofágy provádějí makroendocytózu a efferocytózu larválních adipocytů (Ghosh, Ghosh and Mandal, 2020). Překvapivé je, že role makrofágů během metamorfózy se zdála být obecně naprosto nedůležitou, jelikož jejich genetická ablace měla zanedbatelný vliv jak na průběh metamorfózy, tak na následné vykuklení dospělce (Nelliot, Bond and Hoshizaki, 2006).

Tato práce si dává za cíl zmapovat procesy na úrovni larválních adipocytů a makrofágů probíhající v larválním tukovém tělese během metamorfózy a post-metamorfického vývoje drosophily a objasnit tak roli infiltrujících imunitních buněk během tohoto období za využití mikroskopických metod a moderních přístupů molekulární biologie.

Naše výsledky ukazují, že makrofágy během období kukly a raného post-metamorfického života dospělce hrají naprosto zásadní roli v metabolismu a redistribuci nutrientů. Prokázali jsme, že kromě efferocytózy adipocytů makrofágy infiltrující larvální tukové těleso zachytávají také unikající lipidové kapky a RNP granule z histolyzujícího tukového tělesa, což vede ke vzniku „foamy“ fenotypu. Makrofágy pak recyklují tyto nutrienty a produkují lipophoriny, které jsou nezbytné pro brzkou maturaci orgánů a tkání dospělce, jako jsou například ovaria, a přispívají tak k reprodukčnímu fitness čerstvě vylíhnutých dospělců.

Seznam použité literatury:

Aguila, J. R. *et al.* (2007) 'The role of larval fat cells in adult Drosophila melanogaster', *Journal of Experimental Biology*, 210(6), pp. 956–963. doi: 10.1242/jeb.001586.

Azeez, O. I., Meintjes, R. and Chamunorwa, J. P. (2014) 'Fat body, fat pad and adipose tissues in invertebrates and vertebrates: the nexus', *Lipids in Health and Disease*, 13(1), p. 71. doi: 10.1186/1476-511X-13-71.

Bond, N. D. *et al.* (2011) 'ßFTZ-F1 and Matrix metalloproteinase 2 are required for fat-body remodeling in Drosophila', *Developmental Biology*, 360(2), pp. 286–296. doi: 10.1016/j.ydbio.2011.09.015.

ten Brink, H., de Roos, A. M. and Dieckmann, U. (2019) 'The Evolutionary Ecology of Metamorphosis', *The American Naturalist*, 193(5), pp. E116–E131. doi: 10.1086/701779.

Briegel, H. (1990) 'Metabolic relationship between female body size, reserves, and fecundity of Aedes aegypti', *Journal of Insect Physiology*, 36(3), pp. 165–172. doi: 10.1016/0022-1910(90)90118-Y.

Butterworth, F. M., Emerson, L. and Rasch, E. M. (1988) 'Maturation and degeneration of the fat body in the Drosophila larva and pupa as revealed by morphometric analysis', *Tissue and Cell*, 20(2), pp. 255–268. doi: 10.1016/0040-8166(88)90047-X.

Cinti, S. *et al.* (2005) 'Adipocyte death defines macrophage localization and function in adipose tissue of obese mice and humans', *Journal of Lipid Research*, 46(11), pp. 2347–2355. doi: 10.1194/jlr.M500294-JLR200.

Dai, J. *et al.* (2017) 'Inter-adipocyte Adhesion and Signaling by Collagen IV Intercellular Concentrations in Drosophila', *Current Biology*, 27(18), pp. 2729-2740.e4. doi: 10.1016/j.cub.2017.08.002.

Danielová, A., 2021: Charakteristika přeměny larvální tukové tkáně v průběhu metamorfózy u Drosophila melanogaster [Characterization of remodeling of larval adipose tissue during the metamorphosis of Drosophila melanogaster. Master Thesis, in Czech] – 56 p., Faculty of Science, University of South Bohemia, České Budějovice, Czech Republic.

D'Avino, P. P. and Thummel, C. S. (2000) 'The Ecdysone Regulatory Pathway Controls Wing Morphogenesis and Integrin Expression during Drosophila Metamorphosis', *Developmental Biology*, 220(2), pp. 211–224. doi: 10.1006/dbio.2000.9650.

Franc, N. C. *et al.* (1996) 'Croquemort, A Novel Drosophila Hemocyte/Macrophage Receptor that Recognizes Apoptotic Cells', *Immunity*, 4(5), pp. 431–443. doi:

10.1016/S1074-7613(00)80410-0.

Ghosh, Saikat, Ghosh, Sushmit and Mandal, L. (2020) 'Drosophila metamorphosis involves hemocyte mediated macroendocytosis and efferocytosis', *The International Journal of Developmental Biology*, 64(4-5–6), pp. 319–329. doi: 10.1387/ijdb.190215lm.

Haka, A. S. *et al.* (2016) 'Exocytosis of macrophage lysosomes leads to digestion of apoptotic adipocytes and foam cell formation', *Journal of Lipid Research*, 57(6), pp. 980–992. doi: 10.1194/jlr.M064089.

Jouni, Z. E., Zamora, J. and Wells, M. A. (2002) 'Absorption and tissue distribution of cholesterol in Manduca sexta', *Archives of Insect Biochemistry and Physiology*, 49(3), pp. 167–175. doi: 10.1002/arch.10017.

KAMBYSELLIS, M. P. (1977) 'Genetic and Hormonal Regulation of Vitellogenesis in Drosophila', *American Zoologist*, 17(3), pp. 535–549. doi: 10.1093/icb/17.3.535.

Locke, M. and Collins, J. V. (1965) 'THE STRUCTURE AND FORMATION OF PROTEIN GRANULES IN THE FAT BODY OF AN INSECT', *The Journal of Cell Biology*, 26(3), pp. 857–884. doi: 10.1083/jcb.26.3.857.

Nelliot, A., Bond, N. and Hoshizaki, D. K. (2006) 'Fat-body remodeling in Drosophila melanogaster', *genesis*, 44(8), pp. 396–400. doi: 10.1002/dvg.20229.

Palm, W. *et al.* (2012) 'Lipoproteins in Drosophila melanogaster—Assembly, Function, and Influence on Tissue Lipid Composition', *PLoS Genetics*. Edited by R. P. Kühnlein, 8(7), p. e1002828. doi: 10.1371/journal.pgen.1002828.

Poças, G. M., Crosbie, A. E. and Mirth, C. K. (2022) 'When does diet matter? The roles of larval and adult nutrition in regulating adult size traits in Drosophila melanogaster', *Journal of Insect Physiology*, 139, p. 104051. doi: 10.1016/j.jinsphys.2020.104051.

Regan, J. C. *et al.* (2013) 'Steroid Hormone Signaling Is Essential to Regulate Innate Immune Cells and Fight Bacterial Infection in Drosophila', *PLoS Pathogens*. Edited by D. S. Schneider, 9(10), p. e1003720. doi: 10.1371/journal.ppat.1003720.

Rehman, N. and Varghese, J. (2021) 'Larval nutrition influences adult fat stores and starvation resistance in Drosophila', *PLOS ONE*. Edited by K.-J. Min, 16(2), p. e0247175. doi: 10.1371/journal.pone.0247175.

Rode, S. *et al.* (2018) 'Differential Requirement for Translation Initiation Factor Pathways during Ecdysone-Dependent Neuronal Remodeling in Drosophila', *Cell Reports*, 24(9), pp. 2287-2299.e4. doi: 10.1016/j.celrep.2018.07.074.

Schmitz, G. and Müller, G. (1991) ‘Structure and function of lamellar bodies, lipid-protein complexes involved in storage and secretion of cellular lipids.’, *Journal of lipid research*, 32(10), pp. 1539–70. Available at: http://www.ncbi.nlm.nih.gov/pubmed/1797938.

Storelli, G. *et al.* (2019) ‘Drosophila HNF4 Directs a Switch in Lipid Metabolism that Supports the Transition to Adulthood’, *Developmental Cell*, 48(2), pp. 200-214.e6. doi: 10.1016/j.devcel.2018.11.030.

Tapadia, M. G. and Verma, P. (2012) ‘Immune Response and Anti-Microbial Peptides Expression in Malpighian Tubules of Drosophila melanogaster Is under Developmental Regulation’, *PLoS ONE*. Edited by M. Kango-Singh, 7(7), p. e40714. doi: 10.1371/journal.pone.0040714.

Tysell, B. and Butterworth, F. M. (1978) ‘Different rate of protein granule formation in the larval fat body of Drosophila melanogaster’, *Journal of Insect Physiology*, 24(3), pp. 201–206. doi: 10.1016/0022-1910(78)90035-5.

Vilmos, P. (1998) ‘Insect immunity: evolutionary roots of the mammalian innate immune system’, *Immunology Letters*, 62(2), pp. 59–66. doi: 10.1016/S0165-2478(98)00023-6.

Gabriela Krejčová, Adéla Danielová, Hana Sehadová, Filip Dyčka, Jiří Kubásek, Martin Moos, Adam Bajgar (2024): Macrophages play a nutritive role in post-metamorphic maturation in *Drosophila*. Development. 151(7):dev202492. doi: 10.1242/dev.202492.

Abstract:
In the body of multicellular organisms, macrophages play an indispensable role in maintaining tissue homeostasis by removing old, apoptotic and damaged cells. In addition, macrophages allow significant remodeling of body plans during embryonic morphogenesis, regeneration and metamorphosis. Although the huge amount of organic matter that must be removed during these processes represents a potential source of nutrients, their further use by the organism has not yet been addressed. Here, we document that, during metamorphosis, Drosophila larval adipose tissue is infiltrated by macrophages, which remove dying adipocytes by efferocytosis and engulf leaking RNA-protein granules and lipids. Consequently, the infiltrating macrophages transiently adopt the adipocyte-like metabolic profile to convert remnants of dying adipocytes to lipoproteins and storage peptides that nutritionally support post-metamorphic development. This process is fundamental for the full maturation of ovaries and the achievement of early fecundity of individuals. Whether macrophages play an analogous role in other situations of apoptotic cell removal remains to be elucidated.

© 2024. Published by The Company of Biologists Ltd | Development (2024) 151, dev202492. doi:10.1242/dev.202492

RESEARCH ARTICLE

Macrophages play a nutritive role in post-metamorphic maturation in *Drosophila*

Gabriela Krejčová[1,*], Adéla Danielová[1], Hana Sehadová[2], Filip Dyčka[3], Jiří Kubásek[4], Martin Moos[2] and Adam Bajgar[1,2,*]

ABSTRACT

In the body of multicellular organisms, macrophages play an indispensable role in maintaining tissue homeostasis by removing old, apoptotic and damaged cells. In addition, macrophages allow significant remodeling of body plans during embryonic morphogenesis, regeneration and metamorphosis. Although the huge amount of organic matter that must be removed during these processes represents a potential source of nutrients, their further use by the organism has not yet been addressed. Here, we document that, during metamorphosis, *Drosophila* larval adipose tissue is infiltrated by macrophages, which remove dying adipocytes by efferocytosis and engulf leaking RNA-protein granules and lipids. Consequently, the infiltrating macrophages transiently adopt the adipocyte-like metabolic profile to convert remnants of dying adipocytes to lipoproteins and storage peptides that nutritionally support post-metamorphic development. This process is fundamental for the full maturation of ovaries and the achievement of early fecundity of individuals. Whether macrophages play an analogous role in other situations of apoptotic cell removal remains to be elucidated.

KEY WORDS: *Drosophila* macrophages, Efferocytosis, Metamorphosis, Macrophage metabolic polarization, Post-metamorphic maturation, Lipoproteins

INTRODUCTION

A continuous cycle of removing senescent, damaged and apoptotic cells and replacing them with new ones is essential for the health of all multicellular organisms (Doran et al., 2020). The number of dying cells in a healthy organism reaches tens of billions every day, and their removal is therefore essential to maintain tissue homeostasis (Elliott and Ravichandran, 2016). Macrophages play a key role in this process. Senescent, damaged and apoptotic cells produce characteristic signals that allow their recognition and removal by a process called efferocytosis (Elliott and Ravichandran, 2016). Although the mechanism by which macrophages recognize and engulf these cells is well understood (Hochreiter-Hufford and Ravichandran, 2013), it is unclear whether and how the remnants of the disposed cells are handled in the organism. It can be assumed that the structural components of the engulfed apoptotic cells are further recycled and reused by the organism to avoid wasting the nutrients and building blocks. To this end, the matter of the dying cellular debris must be converted into a form of nutrients suitable for transport, storage or direct use. This phenomenon can be expected to be particularly important in situations where certain tissues undergo massive remodeling, such as embryonic morphogenesis, regeneration or metamorphosis (Ghosh et al., 2020; Mezu-Ndubuisi and Maheshwari, 2021).

Holometabolous insects have periods of growth and nutrient accumulation that are ecologically separated from periods of reproductive activity. Because these two stages are connected with different ecological requirements, individuals must undergo a major transformation of their body plan during complete metamorphosis. In this process, the majority of larval tissues undergo histolysis and most adult structures emerge from the imaginal discs (ten Brink et al., 2019). This poses a fundamental problem to the individual of how to transfer nutrient and energy reserves from the larval to the adult life stage.

In growing larvae, energy-rich carbohydrates, lipids and storage peptides are stored primarily in the central metabolic organ, the fat body, and in the circulating hemolymph (Poças et al., 2022). At the onset of metamorphosis, the peak of the steroid hormone ecdysone triggers preparation for the upcoming period of nutrient scarcity (Juarez-Carreño et al., 2021). The storage peptides and carbohydrates from the hemolymph are resorbed into the polytene adipocytes of the fat body, where they, together with abundant mRNA transcripts and organelles such as endoplasmic reticulum and mitochondria, give rise to ribonucleoprotein granules (RNP granules) (Locke and Collins, 1965; Tysell and Butterworth, 1978; Butterworth et al., 1988; Bond et al., 2011). Thus, the adipocytes become hypertrophic and the fat body is massively infiltrated by larval macrophage-like cells called plasmatocytes (Nelliot et al., 2006; Franz et al., 2018; Ghosh et al., 2020; Tsuyama et al., 2023). However, publications investigating the role of macrophages in the whole process are relatively scarce and the macrophage role in adipose tissue remodeling is considered of negligible importance (Nelliot et al., 2006).

Nutrients stored in adipocytes are not significantly used during metamorphosis and serve predominantly for the emergence and post-metamorphic maturation of the reproductive organs, the formation of adult fat reserves and cuticle tanning (Aguila et al., 2007; Storelli et al., 2019). Therefore, all stores from adipocytes are fully used during the first 72 h of adult *Drosophila* life, and larval adipocytes are completely depleted during this short period (Rehman and Varghese, 2021). Although larval fat body reserves are essential for these processes, the mechanism of nutrient mobilization from histolysis-undergoing adipocytes has not yet

[1]Department of Molecular Biology and Genetics, Faculty of Science, University of South Bohemia, Ceske Budejovice, 37005, Czech Republic. [2]Institute of Entomology, Biology Centre of the Czech Academy of Sciences, Ceske Budejovice, 37005, Czech Republic. [3]Department of Chemistry, Faculty of Science, University of South Bohemia, Ceske Budejovice, 37005, Czech Republic. [4]Department of Experimental Plant Biology, Faculty of Science, University of South Bohemia, Ceske Budejovice, 37005, Czech Republic.

*Authors for correspondence (bajgaradam@seznam.cz, krejcovagabriela@seznam.cz)

G.K., 0000-0003-4648-973X; A.B., 0000-0002-9721-7534

Handling Editor: Irene Miguel-Aliaga
Received 1 November 2023; Accepted 27 February 2024

Development (2024) 151, dev202492. doi:10.1242/dev.202492

been revealed. This is of particular interest because the formation of RNP granules together with ribosome sequestration indicates limited translation in the histolyzing adipocytes, while the adult fat body is not yet fully established (Rode et al., 2018). Although the adult fat body precursors start to accumulate lipid droplets already during pupal stages, the process of gradual differentiation of the adult fat body precursors into mature adult adipocytes is complete at day 2 after eclosion of the adult, and hence the individual must overcome this metabolically sensitive period without any fully functional central metabolic organ (Lei et al., 2023; Tsuyama et al., 2023).

The mutual interactions between macrophages and adipocytes have been most studied in the pathogenesis of obesity and metabolic syndrome (Li et al., 2020). Hypertrophic adipose tissue in obese individuals is heavily infiltrated by macrophages, which form characteristic crown-like structures around adipocytes and, in response to excessive lipid intake, become foamy and significantly increase their ability to process engulfed lipids (Aouadi et al., 2014; Dahik et al., 2020). This phenomenon is not exclusively connected with obesity and the adipose tissue also appears to be infiltrated by macrophages in other stressful situations such as starvation, infection or congenital dyslipidemia; however, their role under these circumstances remains enigmatic (Kosteli et al., 2010; Silva et al., 2019).

We have shown that the larval fat body of *Drosophila* is massively infiltrated during metamorphosis by macrophages that take up lipids and RNP granules from dying adipocytes. Infiltrating macrophages display many of the characteristics of adipocytes at the transcriptomic, proteomic and morphological levels and significantly participate in the processing and redistribution of nutrients from the histolyzing adipocytes that nutritionally support post-metamorphic maturation and female fecundity.

RESULTS

Macrophages participate in adipose tissue remodeling during insect metamorphosis

To understand the mechanism of nutrient mobilization for post-metamorphic maturation, we first characterized the progress of fat body remodeling at the level of its ultrastructure over the course of metamorphosis. Initially, the fat body of third instar larvae consists of polygonal sheet-like cells with cytosol filled predominantly with lipid droplets. At the onset of metamorphosis, however, the individual adipocytes become more spherical and resorb storage peptides and carbohydrates from the circulation into the cytosol, thereby becoming hypertrophic. Confocal microscopy analysis of flies bearing the *croquemort-GFP* construct, which is specifically expressed in macrophages, revealed that as the metamorphosis proceeds and larval fat body disintegrates, macrophages infiltrate this tissue and closely interact with hypertrophic adipocytes (Fig. 1A; Fig. S1A).

Resorbed storage peptides accumulate in the cytosol where, together with autophagy of the rough endoplasmic reticulum and other cytosolic organelles, they give rise to a matter which later condenses into electron-dense RNA-protein granules (Fig. 1B; Fig. S1B) (Butterworth et al., 1988), which are strongly autofluorescent (Fig. 1A). Whereas at the onset of metamorphosis, the organelles still can be distinguished within the RNP granules (Fig. 1C), later, the RNP granules become denser, contain a urate crystalline core (Locke and Collins, 1965) (Fig. 1D) and fuse into the granules of larger diameter (Fig. 2A).

Although changes in the ultrastructure of adipocytes are rather gradual over the course of metamorphosis, the remodeling of the fat body accelerates dramatically around the time of emergence. Use of nutrients from the larval adipocytes is essential for successful metamorphosis, as flies carrying the adipocyte-specific overexpression of the dominant-negative form of the ecdysone receptor are unable to form RNP granules and exhibit a significant mortality rate at emergence (Fig. S1C,D,E).

During the first 48 h post-eclosion, the number of RNP granules in the cytosol of adipocytes decreases significantly (Fig. 2B). This decrease can be attributed to the disintegration of granules in adipocyte cytosol, as deliberated endoplasmic reticulum with dilated cisternae and other organelles suddenly appear in close vicinity of the plasma membrane (Fig. 2C) and in extracellular space (Fig. 2D). RNP granules also disintegrate to some extent via budding, as previously described (Locke and Collins, 1965) (Fig. 2E). Additionally, whole RNP granules and lipid droplets can be observed in the extracellular space (Fig. 2F,G).

As the number of RNP granules within adipocytes decreases (Fig. 2B), it eventually leads to the occurrence of adipocytes filled only with lipid droplets (Fig. S2A). Along with the release of nutrients, adipocytes gradually decrease in diameter and eventually disappear entirely during the first 72 h of post-metamorphic development (Fig. 2H,I). Notably, the matter from adipocytes can be observed in the cytosol of the infiltrating macrophages (Fig. S2B,C). Although previous work has suggested that macrophages play a negligible role in adipose tissue remodeling in *Drosophila* (Nelliot et al., 2006), our data show that previously used genetic tools for their depletion are not fully functional and do not lead to a significant limitation of macrophage function. Although macrophage-specific overexpression of *hid* and *rpr* results in quenching of the GFP signal (Fig. S3A), microscopy analysis of adipose tissue dissected from freshly emerged female virgins revealed that cells displaying macrophage morphology still persist in this tissue. Moreover, these cells form the typical crown-like structures around the adipocytes as in controls (Fig. S3B) and stain for the macrophage-specific anti-NimC1 antibody (Fig. S3C), a scavenger receptor that mediates phagocytosis of bacteria. Indeed, these cells are capable of phagocytosis, as documented by injection of heat-killed *Staphylococcus aureus* conjugated to the pH-sensitive dye pHrodo (Fig. S3D). The macrophages also exhibit the ability to spread when placed on a microscopic slide (Fig. S3E), thus documenting their viability.

The conclusion that genetic constructs traditionally used for macrophage ablation do not induce apoptosis in these cells was drawn by Stephenson and colleagues (Stephenson et al., 2022). In addition, using a newly established line of macrophage-specific Gal4 driver ($Hml^{e9\text{-}P2a}$ Gal4), they demonstrated that macrophages play an indispensable role during metamorphosis (Stephenson et al., 2022). Their data are in congruence with our observations that flies with macrophage-specific overexpression of the pro-apoptotic protein *grim* using the $Hml^{e9\text{-}P2a}$ Gal4 driver line (Stephenson et al., 2022) die shortly after the pre-pupa-to-pupa transition and display certain morphological abnormalities. In particular, these pupae lack visible anterior spiracles, and do not undergo the head eversion otherwise observed in pupal stage P4 (Fig. 3A). Moreover, the body cavity of these individuals contains the debris of non-phagocytosed larval muscles (Fig. 3B) and less disintegrated larval fat body compared with controls (Fig. 3C).

To overcome lethality at this stage of metamorphosis, the construct used for ablation of macrophages was activated after pupal stage P8 by combining a macrophage-specific driver with a temperature-sensitive inhibitor protein ($Hml^{e9\text{-}P2a}$ Gal4, Tub

Development (2024) 151, dev202492. doi:10.1242/dev.202492

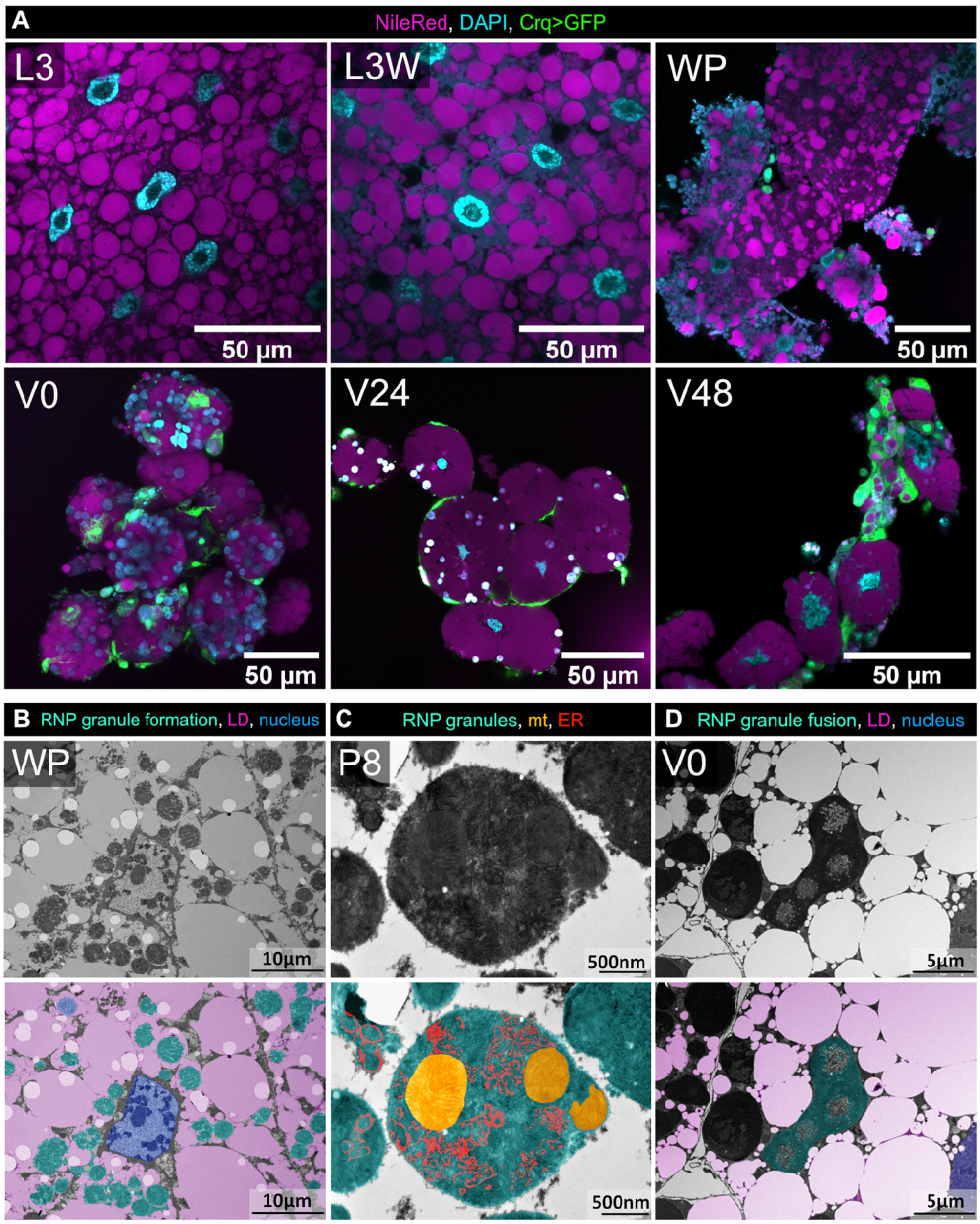

Fig. 1. The progress of fat body remodeling during metamorphosis and post-metamorphic maturation. (A) Representative confocal images documenting the onset of fat body disintegration (WP), infiltration of macrophages (*Crq>GFP*; green) and formation of RNA-protein granules (autofluorescence; cyan). Lipids were stained by NileRed (magenta), DAPI marks nuclei (cyan). (B) Representative transmission electron micrograph documenting the formation of RNA-protein granules around the adipocyte nucleus. (C) Representative transmission electron micrograph showing RNA-protein granules in which autophagocytosed mitochondria and ribosomes can be distinguished. (D) Representative transmission electron micrograph documenting fusion of the RNA-protein granules, which contain a crystalline core. In B-D: cyan pseudocoloring depicts RNA-protein granules; blue, nuclei; magenta, lipid droplets (LD); yellow, mitochondria (mt); red, ribosomes. L3, late 3rd instar larvae; L3W, wandering 3rd instar larvae; P8, pupal stage 8; V0, freshly emerged fly; V24, 1-day-old virgin; V48, 2-day-old virgin; WP, white prepupa.

Gal80^{TS}; see Fig. S3G,H for efficiency of macrophage ablation and Fig. S3I,J for colocalization of *Hml* and *Crq* macrophage Gal4 drivers). Delayed ablation of macrophages allows the individuals to finish metamorphosis even without these cells at the time of emergence. However, the emerged individuals display abnormal post-metamorphic maturation, as they have significantly delayed ovarian development (Fig. 3D,E) and are unable to expand their wings (Fig. 3F), as suggested in a previous study (Kiger et al., 2001).

Given that the entire fat body mass of larvae, which constitutes about 23% of the body of newly emerged virgins, completely disappears during the first 3 days after emergence (Fig. 2I; Figs S1F and S2D; Movies 1,2,3), we assume an extremely rapid redistribution of nutrients. We decided to inspect the macrophage role in this process, as the data presented above document their infiltration into adipose tissue and their importance for post-metamorphic maturation (Figs 1A and Fig. 3D-F; Fig. S1A).

Macrophages transiently acquire adipocyte-like metabolic features

Further examination of macrophages infiltrating adipose tissue revealed a surprisingly close interaction between macrophages and adipocytes. Confocal imaging of the larval adipose tissue dissected from freshly emerged flies bearing the *Crq>GFP* construct revealed that the macrophages form crown-like structures around the hypertrophic adipocytes (Fig. 4A; Fig. S4A) and cover a significant portion of their surface (Fig. 4B,C; Fig. S4B). Infiltrating macrophages intercalate their lamellipodia into the adipocytes with disrupted plasma membrane and clear either fragments or whole depleted cells via efferocytosis (Fig. 4D).

Transmission electron microscopy revealed that macrophages show signs of increased processing of lipids, RNP granules and other cellular debris. The RNP complexes may be found abundantly in the cytosol of infiltrating macrophages as leaking RNP granules are endocytosed and subsequently untangled by these cells

Development (2024) 151, dev202492. doi:10.1242/dev.202492

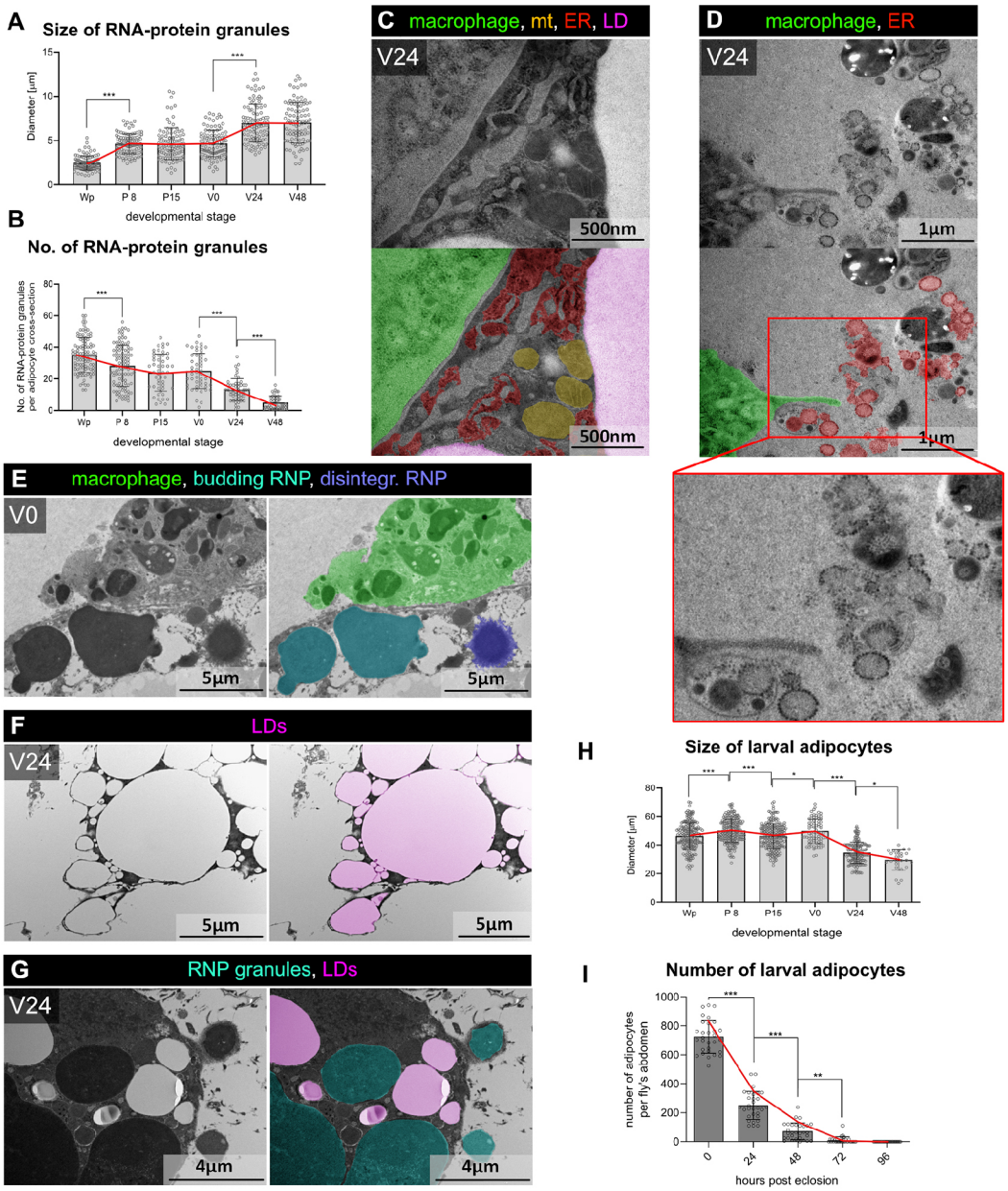

Fig. 2. The changes in the fat body morphology and ultrastructure during metamorphosis. (A) The diameter of RNA-protein granules in adipocytes in the course of metamorphosis. (B) Number of RNA-protein granules per adipocyte cross-section (section plane across the adipocyte nucleus) in the course of metamorphosis. (C,D) Representative transmission electron micrograph showing the deliberated endoplasmic reticulum (ER) and mitochondria (mt) in the cytosol of the adipocyte (C) and in extracellular space (D). (E) Representative transmission electron micrograph documenting disintegration of the RNA-protein granules at 24 h post eclosion via budding of the granules or dissolving. (F,G) Lipids (F) and RNA-protein granules (G) leaking from the histolyzing adipocytes. (H) Diameter of larval adipocytes in the course of metamorphosis. (I) Number of larval adipocytes per abdomen of flies at respective time points after emergence. Data in A, B and H were quantified from histological sections of five flies stained by Mallory trichrome staining and the results were compared using one-way ANOVA. The dots represent individual values with a line/bar showing mean±s.d. Asterisks mark statistically significant differences (*P<0.05; **P<0.01; ***P<0.001). In pseudocolored TEM images: magenta, lipid droplets (LD); green, macrophages; red, ribosomes; yellow, mitochondria; cyan, RNA-protein granules; blue, disintegrating RNA-protein granules. P8, pupal stage 8; P15, pupal stage 16; V0, freshly emerged fly; V24, 1-day-old virgin; V48, 2-day-old virgin; Wp, white prepupa.

(Fig. 4E,F; Fig. S2C). Excessive lipid uptake and efferocytosis leads to a frequent occurrence of multilamellar bodies (Fig. 4F; Fig. S4C), structures attributed to lysosomal processing and storage of polar lipids (Schmitz and Muller, 1991). Eventually, the infiltrating macrophages are reminiscent of foamy macrophages known from obese mammals and closely resemble adipocytes themselves in their ultrastructure (Fig. 4G; Fig. S4D,E). Lipidomics analysis showed that the macrophages isolated from freshly emerged virgins have significantly increased levels of total lipids when compared with macrophages from larval stage L3W (Fig. 5A; Table S1). This observation is further supported by elevated cholesterol and cholesteryl-ester levels during metamorphosis and early post-metamorphic development (Fig. S4F). As the post-metamorphic development proceeds and the adipocytes slowly disappear, the

Development (2024) 151, dev202492. doi:10.1242/dev.202492

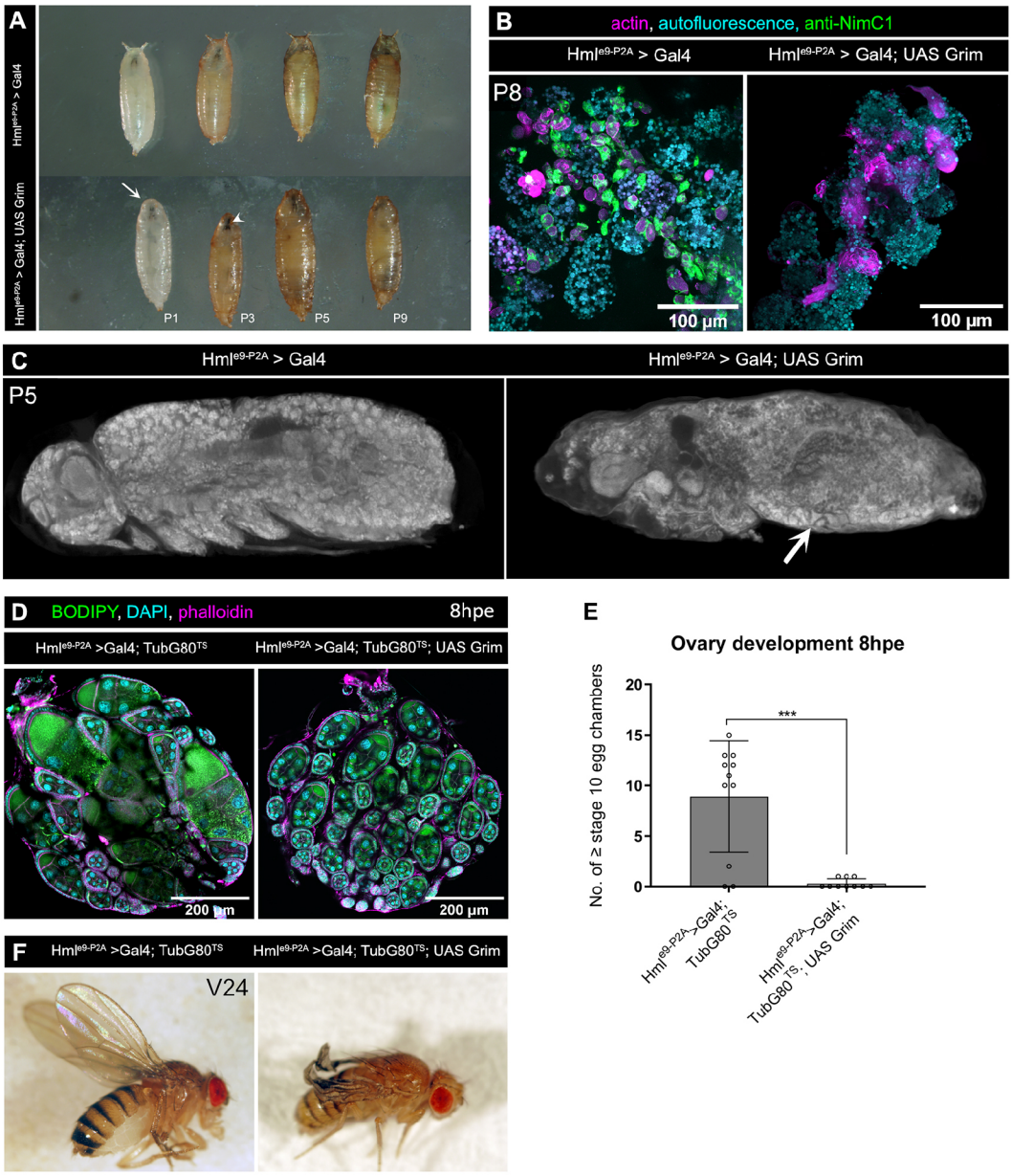

Fig. 3. Macrophages are indispensable for successful metamorphosis. (A) Representative images of control pupae (*Hml$^{e9\text{-}P2A}$-GAL4*; upper row) and pupae bearing the *Hml$^{e9\text{-}P2A}$-GAL4>UAS Grim* genetic construct (lower row). Arrow marks missing anterior spiracles, arrowhead shows lacking head eversion. (B) Representative confocal images depicting the presence of non-phagocytosed debris of larval muscles (visualized by Phalloidin, magenta) dissected from pupae bearing the *Hml$^{e9\text{-}P2A}$-GAL4>UAS Grim* genetic construct compared with the controls, in which the muscle debris is engulfed by macrophages. Autofluorescence is shown in a cyan channel. (C) Reconstructed micro-computed tomography images of control pupae (*Hml$^{e9\text{-}P2A}$-GAL4*; left) and pupae bearing the *Hml$^{e9\text{-}P2A}$-GAL4>UAS Grim* genetic construct (right). The arrow shows debris of non-phagocytosed larval muscles.
(D) Representative confocal images of ovaries dissected from flies bearing the *Hml$^{e9\text{-}P2A}$-GAL4>TubGal80^{TS}*; *UAS Grim* genetic construct (right), depicting their delayed development compared with controls (left) at 8 h post eclosion (hpe). (E) Number of egg chambers reaching the developmental stage 10 and older in control individuals (*Hml$^{e9\text{-}P2A}$-GAL4>TubGal80^{TS}*) and flies with genetically ablated macrophages (*Hml$^{e9\text{-}P2A}$-GAL4>TubGal80^{TS}*; *UAS Grim*) at 8 hpe. The dots represent individual values with a line/bar showing mean±s.d. ***P<0.001 (unpaired, two-tailed Student's t-test). (F) Representative images of flies bearing the *Hml$^{e9\text{-}P2A}$-GAL4>TubGal80^{TS}*; *UAS Grim* genetic construct (right), depicting their inability of wing expansion compared with controls (left) at 24 hpe. P1, pupal stage P1; P3, pupal stage P3; P5, pupal stage P5; P9, pupal stage P9; V24, 1-day-old virgin.

percentage of macrophage cytosol occupied by lipid droplets increases substantially (Fig. 5B,C). The lipidomic profile of macrophages isolated from freshly emerged flies is shifted toward an increased abundance of polar lipids and ceramides when compared with adipocytes in terms of composition and prevalence of lipid species (Fig. 5D; Tables S1 and S2).

Transcriptomic profiling of macrophages isolated from newly emerged virgin flies revealed that these cells primarily increase the expression of genes involved in the synthesis of energy-rich metabolites and their precursors. In particular, the genes involved in lipid metabolism and lipoprotein biosynthetic processes are significantly upregulated in these cells compared with macrophages

Development (2024) 151, dev202492. doi:10.1242/dev.202492

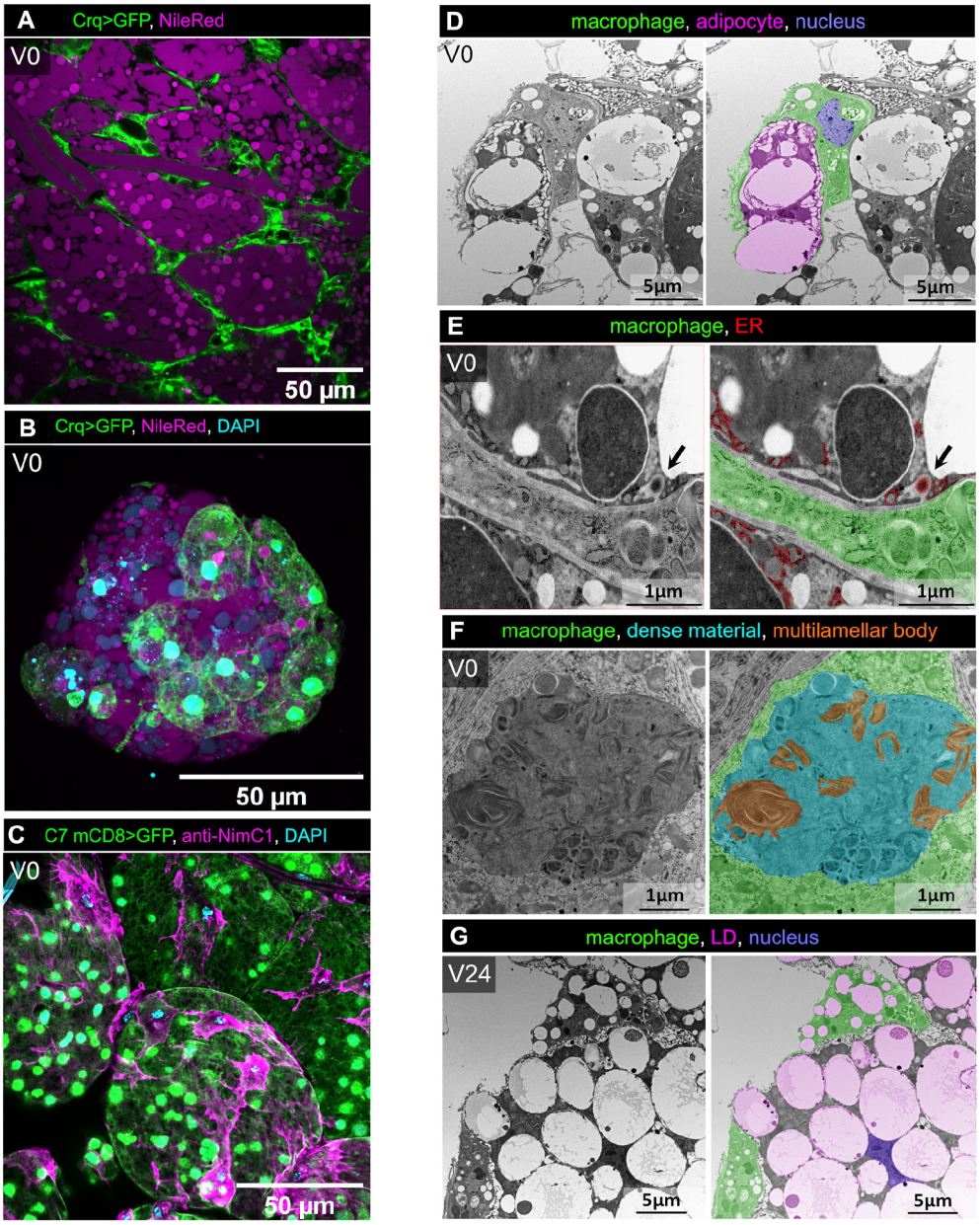

Fig. 4. Macrophages heavily infiltrate the larval fat body during metamorphosis. (A) Representative confocal image showing the crown-like structures formed by infiltrating macrophages (*Crq>GFP*). Lipids were stained by NileRed (magenta). Lighter magenta spheres are the RNA-protein granules. (B) Representative confocal image of dissected individual larval adipocyte with attached macrophages (*Crq>GFP*; green). Lipids were stained by NileRed (magenta), DAPI marks nuclei (cyan). Autofluorescence of the RNA-protein granules in cyan. From a *z*-stack of seven layers. (C) Representative confocal image of the dissected adipocytes (*C7 mCD8>GFP*; green). The infiltrating macrophages were stained by anti-NimC1 (magenta); nuclei by DAPI (cyan). From a *z*-stack of seven layers. (D) Representative transmission electron micrograph showing efferocytosis of an adipocyte with damaged plasma membrane by a macrophage. (E) Representative transmission electron micrograph depicting the transport of dilated cisternae of endoplasmic reticulum from the adipocyte to the macrophage (arrow). (F) Representative transmission electron micrograph documenting the presence of electron-dense material with multilamellar bodies in a macrophage. (G) Representative transmission electron micrograph of an adipocyte with attached foamy macrophages. In pseudocolored TEM images – macrophages in green, ribosomes in red, electron-dense material in cyan, multilamellar bodies in orange, lipid droplets (LD) in magenta and nuclei in blue. V0, freshly emerged fly; V24, 1-day-old virgin.

isolated from L3W (Fig. 5E; Tables S3, S4 and S5). Targeted analysis showed that macrophages in freshly emerged flies display enhanced expression of genes involved in lipoprotein assembly, production of storage peptides and processing of sphingolipids (Fig. S5A; Tables S3, S4 and S5).

This observation was rather unexpected as these metabolic processes are thought to be almost exclusive to adipocytes. Moreover, many genes strongly elevated in macrophages during post-metamorphic maturation are recognized as characteristic fat body markers (Leader et al., 2018), such as the storage peptides (*Fat body protein 2*, *Larval serum protein 1α* and *Larval serum protein 2*, Odorant-binding proteins) and lipoproteins [*apolipophorin* (*apolpp*), *Apolipoprotein lipid transfer particle*, *Neuropeptide-like precursor 2*] (Fig. S5B; Tables S3, S4 and S5). Nonetheless, in addition to these genes, the macrophages also highly express genes considered to be plasmatocyte markers, such as *croquemort*, *Peroxidasin*, *serpent*, *Hemolectin*, *Nimrod C1* and *eater* (Fig. S5B). Notably, the co-expression of adipocyte- and macrophage-specific markers can be detected only in macrophages isolated from freshly emerged flies, as the adipocyte-like markers are not upregulated in the macrophages isolated from 10-day-old adult flies (Fig. S5B; Tables S3, S4 and S5). These data indicate that, during early post-metamorphic development, macrophages temporarily adopt a unique phenotypic polarization, which comprises the phagocytic capability of macrophages and the metabolic features of adipocytes. Interestingly, their phenotype is reminiscent of adipohemocytes and secreting plasmatocytes identified in recent single-cell RNA-sequencing (RNA-seq) of larval immune cells (Cattenoz et al., 2020; Cho et al., 2020). Indeed, all the identified markers of adipohemocytes and secreting plasmatocytes are expressed at elevated levels in macrophages of newly emerged flies (Fig. S5B; see Fig. S5C for purity of sorted cells).

To confirm this unexpected polarization phenotype, we generated a fly line in which the proteins secreted by macrophages were labeled by ectopic expression of engineered promiscuous biotin ligase (BirA-G3) (Droujinine et al., 2021) in these cells. Proteomic analysis of

Development (2024) 151, dev202492. doi:10.1242/dev.202492

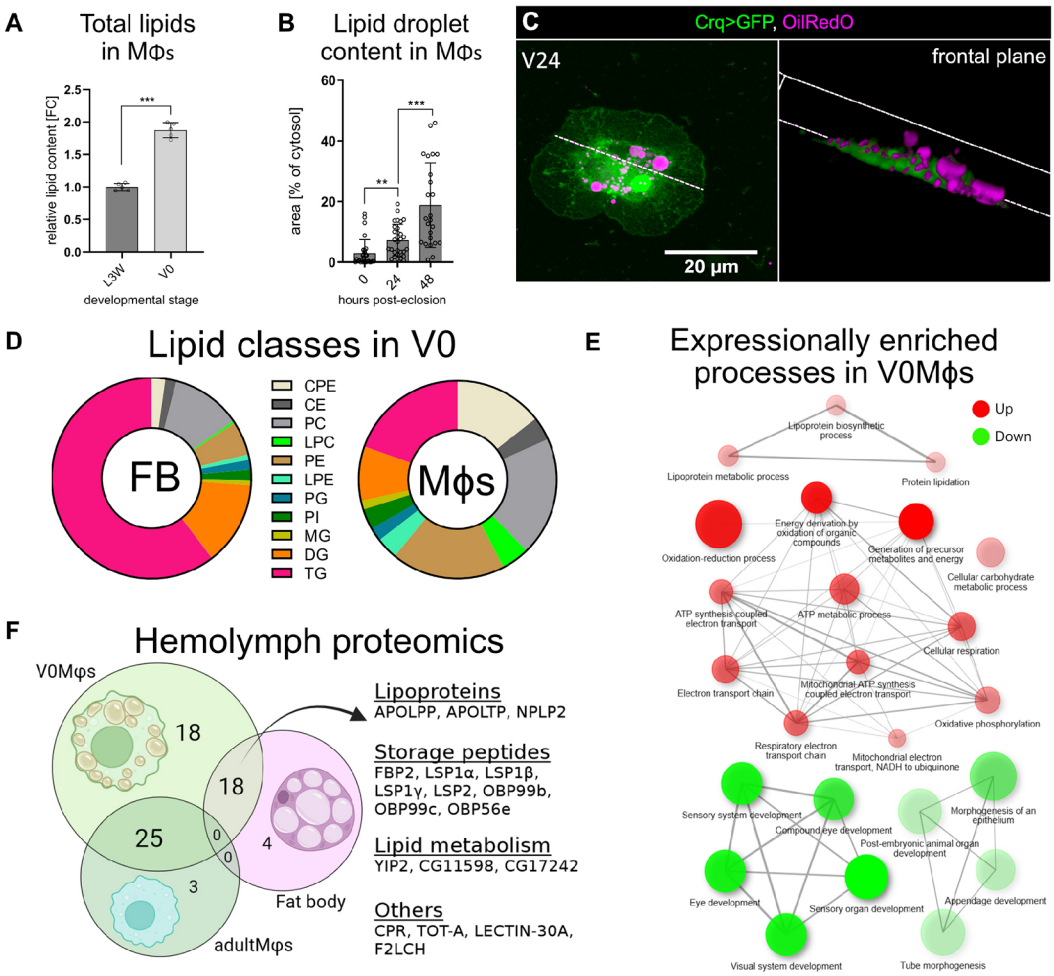

Fig. 5. Macrophages acquire the adipocyte-like metabolic profile during post-metamorphic development. (A) Fold change of relative content of total lipids in macrophages isolated from L3W and V0 as determined by lipidomics analysis. The data were obtained from 90 flies per replicate. Individual dots represent biological replicates with a line/bar showing mean±s.d. (B) Percentage of cytosol occupied by lipid droplets in macrophages isolated at respective time points after emergence. Data were quantified from ten flies per replicate. The data were obtained from three independent experiments. The dots represent values of individual macrophages with a line/bar showing mean±s.d. (C) Representative confocal image of a macrophage (*Crq>GFP*; green) showing accumulation of lipids (NileRed; magenta) in the cytosol. (D) Proportional prevalence of lipid species in the fat body (FB) and macrophages (Mϕs) isolated from V0 as determined by lipidomics analysis. (E) GAGE analysis of transcriptomics data documenting upregulated (red) and downregulated (green) biological processes in macrophages isolated from V0 compared with L3W. (F) Venn diagrams displaying a number of proteins secreted by the adipocytes from L3, macrophages isolated from V0 (V0Mϕs), and adult flies (Mϕs) as determined by proteomics analysis of biotinylated hemolymph fraction (by using tissue-specific overexpression of *BirA(G3)*). ***P*<0.01; ****P*<0.001 (unpaired, two-tailed Student's *t*-test). L3W, wandering 3rd instar larvae; V0, freshly emerged fly; V24, 1-day-old virgin; V48, 2-day-old virgin.

biotinylated proteins isolated from hemolymph confirms our previous notion that macrophages translate and secrete storage peptides and lipoproteins into circulation. We identified 18 macrophage-secreted proteins (predominantly lipoproteins, storage peptides and enzymes involved in lipid metabolism) that are secreted by both macrophages and adipocytes during post-metamorphic maturation, but none of these proteins has been found to be produced by macrophages in fully mature flies (10 days after emergence) (Fig. 5F; Table S6). This indicates that macrophages transiently adopt this unique adipocyte-like polarization to facilitate the mobilization of nutritionally rich substances from the adipocytes.

Production of lipoproteins by macrophages promotes post-metamorphic maturation of ovaries

The presented data show that macrophages facilitate the mobilization of nutrients from larval adipocytes in the form of storage peptides and lipoproteins. We hypothesize that the mobilized nutrients are used for post-metamorphic maturation, which is necessary for rapid adaptation to adult life and reproduction. To investigate the importance of macrophage-mediated nutrient mobilization for this process, we silenced the expression of *apolpp* exclusively in these cells using the macrophage-specific promoter *croquemort* (*Crq>apolpp*^{RNAi}; see Fig. S6A for RNAi efficiency). *Apolpp* represents a major component of lipoproteins in *Drosophila* and is essential for the transport of lipids between tissues (Palm et al., 2012). The expression of *apolpp* in macrophages increases continuously during metamorphosis and peaks 24 h after emergence (Fig. 6A). The production of *apolpp* by macrophages in freshly emerged flies is further documented by the occurrence of a strong GFP signal in these cells in flies bearing the APOLPP-GFP reporter. To a lesser extent, the GFP signal can also be observed on the surface of the RNP granules in larval adipocytes (Fig. 6B), consistent with the proteomic analysis (Fig. 5F).

Development (2024) 151, dev202492. doi:10.1242/dev.202492

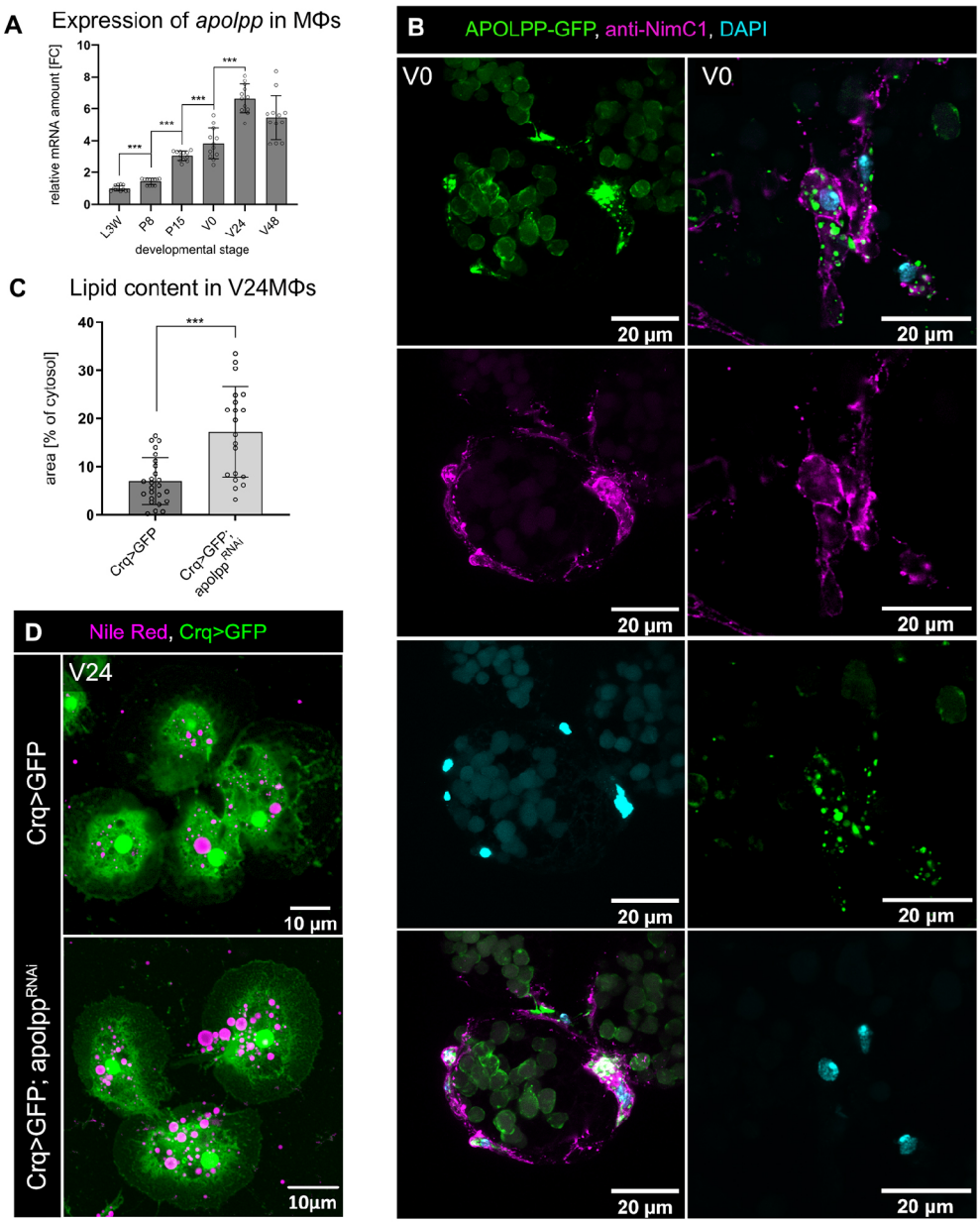

Fig. 6. Macrophages express *apolpp* during the post-metamorphic development. (A) The expression of *apolpp* in macrophages isolated from individuals at respective developmental stages (L3W, P8, P15, V0, V24 and V48). Expression levels normalized against *rp49* are reported as fold change relative to *apolpp* levels in L3W arbitrarily set to 1. Individual dots represent biological replicates with a line/bar showing mean±s.d. ***P<0.001 (one-way ANOVA). (B) Representative confocal images of the larval fat body and infiltrating macrophages stained by the macrophage-specific anti-NimC1 antibody (magenta) dissected from flies bearing the *apolpp-GFP* construct. Nuclei were stained by DAPI (cyan). The image on the right consists of a *z*-stack of eight layers. (C) Percentage of cytosol occupied by lipid droplets in macrophages (Mϕs) isolated from control flies (*Crq>GFP*) and flies with a macrophage-specific *apolpp* knockdown (*Crq>GFP*; *apolpp*^{RNAi}) at V24. Data were quantified from ten flies per replicate. The data were obtained from three independent experiments. The dots represent values of individual macrophages with a line/bar showing mean±s.d. ***P<0.001 (unpaired, two-tailed Student's *t*-test). (D) Representative confocal images of macrophages isolated from control flies (*Crq>GFP*) and flies with a macrophage-specific *apolpp* knockdown (*Crq>GFP*; *apolpp*^{RNAi}). The lipids were stained by NileRed (magenta). L3W, wandering 3rd instar larvae; P8, pupal stage P8; P15, pupal stage P15; V0, freshly emerged fly; V24, 1-day-old virgin; V48, 2-day-old virgin.

The macrophage-specific knockdown of *apolpp* expression leads to an accumulation of neutral lipids in macrophages (Fig. 6C,D). Simultaneously, the macrophage-specific *apolpp* knockdown results in a reduction of lipid deposits in maturing ovaries as manifested by a decrease in free fatty acid (FFA) levels (Fig. 7A; Fig. S6B). Moreover, the amount of ^{13}C-labeled FFAs incorporated into this tissue over the course of metamorphosis is also significantly decreased (Fig. 7B; Fig. S6C). As a consequence, maturation of the ovaries is delayed significantly in these flies. Ovaries of flies with the macrophage-specific *apolpp* knockdown exhibited reduced fluorescence signal of the lipophilic dye (Fig. 7C) and their maturation is significantly delayed (Figs 7D,E; Fig. S6D-F). Accordingly, these females lay fewer eggs during the first 72 h of adult life and exhibit significantly lower fecundity compared with controls (Fig. 7F,G).

The delay in ovary maturation is due to apoptotic regression of maturating egg chambers, as it is observed in adult flies exposed to nutrition scarcity (Barth et al., 2011). An increased level of apoptosis in ovaries has been also previously associated with disruption of sphingolipid metabolism in this tissue (Phan et al., 2007). Nonetheless, the ovaries of flies with macrophage-specific knockdown of *apolpp* do not exhibit any signs of apoptosis (Fig. S7A) and their size is comparable with the controls in 1-week-old flies (Fig. 7H,I), suggesting that silencing of *apolpp* in macrophages can be explained by delayed initiation of ovary maturation at the onset of the adult life stage. In parallel to lipid transport to ovaries, lipids from larval adipocytes are transported to adult fat body tissue formed from an independent cellular lineage. Therefore, we inspected the number of larval adipocytes and morphology of the adult fat body in flies with the macrophage-specific *apolpp* knockdown. Nonetheless, we found no difference either in the number of larval adipocytes during the first 3 days after emergence or in the amount of lipid stores in adult fat body between control flies and flies lacking *apolpp* expression in macrophages (Fig. S7B-D).

Development (2024) 151, dev202492. doi:10.1242/dev.202492

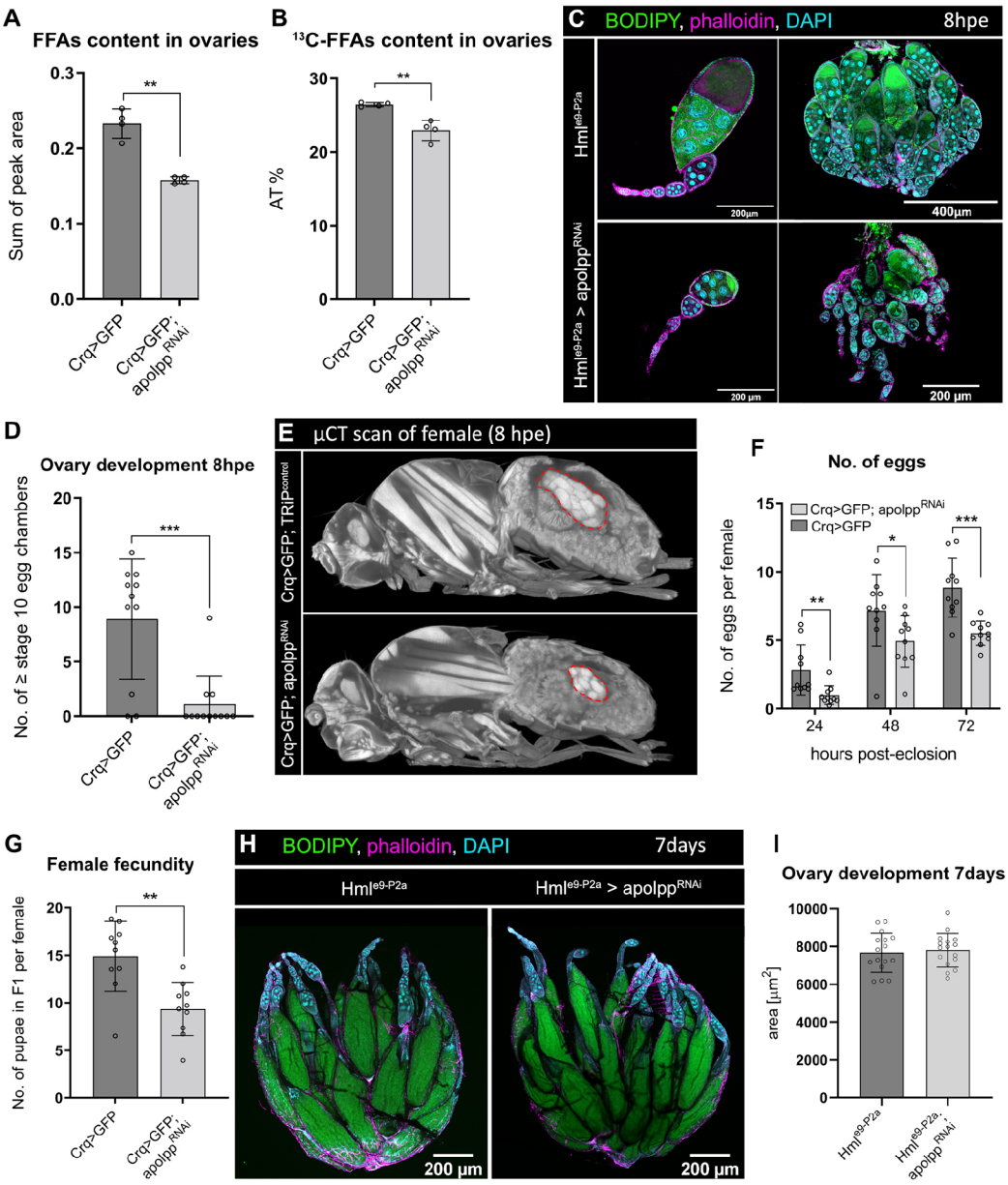

Fig. 7. Macrophages express *apolpp* to ensure the maturation of ovaries. (A) A sum of peak area of free fatty acids measured in ovaries of control individuals (*Crq>GFP*) and flies with macrophage-specific knockdown of *apolpp* (*Crq>GFP*; *apolpp*^{RNAi}) at 8 h post eclosion (hpe). (B) The amount of ^{13}C-labeled free fatty acids (AT%) measured in ovaries of control individuals (*Crq>GFP*) and flies with macrophage-specific knockdown of *apolpp* (*Crq>GFP*; *apolpp*^{RNAi}) at 8 hpe. (C) Representative confocal images of ovarioles (left) and ovaries (right) dissected from control individuals (*Hml*$^{e9\text{-}P2a}$) and flies with macrophage-specific knockdown of *apolpp* (*Hml*$^{e9\text{-}P2a}$; *apolpp*^{RNAi}) at 8 hpe. Lipids were stained by BODIPY (green), actin was labeled by Phalloidin (magenta) and DAPI marks nuclei (cyan). (D) Number of egg chambers reaching the developmental stage 10 and older in control individuals (*Crq>GFP*) and flies with macrophage-specific knockdown of *apolpp* (*Crq>GFP*; *apolpp*^{RNAi}) at 8 hpe. (E) X-ray computed tomography images of control individuals (*Crq>GFP*) and flies with macrophage-specific knockdown of *apolpp* (*Crq>GFP*; *apolpp*^{RNAi}) at 8 hpe with highlighted contour of ovaries (dashed line). (F) An average number of eggs laid by control females (*Crq>GFP*) and flies with macrophage-specific knockdown of *apolpp* (*Crq>GFP*; *apolpp*^{RNAi}) in the first 3 days after emergence. Individual dots display biological replicates (25 females per replicate). (G) An average number of pupae developed from the sum of eggs laid by one female in the first 3 days after emergence by control females (*Crq>GFP*) and flies with macrophage-specific knockdown of *apolpp* (*Crq>GFP*; *apolpp*^{RNAi}). Individual dots display biological replicates (25 females per replicate). (H) Representative confocal images of ovaries dissected from control individuals (*Hml*$^{e9\text{-}P2A}$*-GAL4*) and flies with macrophage-specific knockdown of *apolpp* (*Hml*$^{e9\text{-}P2A}$*-GAL4*; *apolpp*^{RNAi}) at 7 days post eclosion (dpe). Lipids were stained by BODIPY (green), actin was labeled by Phalloidin (magenta) and DAPI marks nuclei (cyan). (I) Size of ovaries dissected from control individuals (*Hml*$^{e9\text{-}P2A}$*-GAL4*) and flies with macrophage-specific knockdown of *apolpp* (*Hml*$^{e9\text{-}P2A}$*-GAL4*; *apolpp*^{RNAi}) at 7 dpe. The dots represent individual values with a line/bar showing mean±s.d. *P<0.05; **P<0.01; ***P<0.001 (unpaired, two-tailed Student's t-test, A,B,D,G,I; one-way ANOVA, F).

Overall, our data demonstrate that the production of APOLPP by macrophages is required for the redistribution of stores during post-metamorphic development and for achieving early ovarian maturation and fecundity (Fig. 8).

DISCUSSION

Macrophages are functionally versatile cells that perform many diverse roles in organisms (Murray and Wynn, 2011). We found that, during *Drosophila* metamorphosis, macrophages infiltrate the larval

Development (2024) 151, dev202492. doi:10.1242/dev.202492

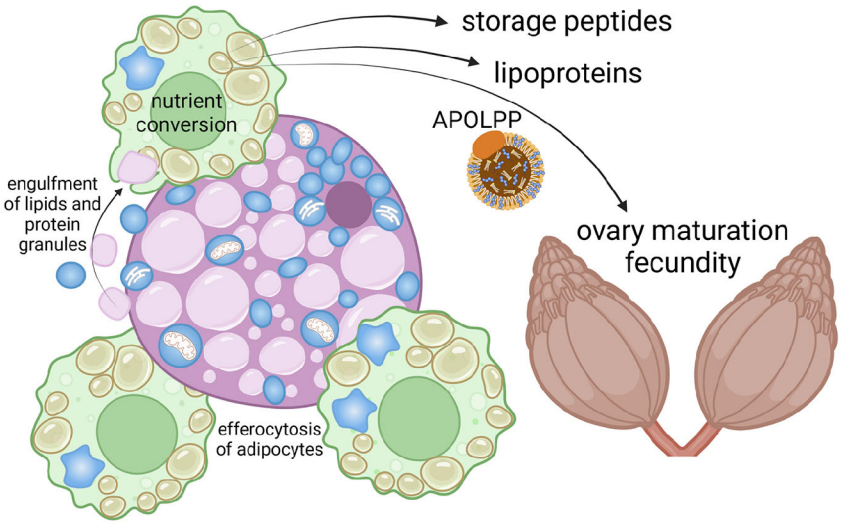

Fig. 8. Schematic representation of the proposed role of macrophages during post-metamorphic maturation in *Drosophila*. Macrophages transiently adopt adipocyte-like properties to convert the mass of dying adipocytes into reusable nutrients, such as storage peptides and lipoproteins, to provide nutrients for ovarian maturation during postmetamorphic development.

adipose tissue and actively participate in the clearance of dying adipocytes and their cellular remnants. The infiltrating macrophages are exposed to an excessive load of leaking lipids, organelles, membranes and RNP granules and undergo a characteristic phenotypic polarization by temporally adopting adipocyte-like features. As the endocytosed cellular matter is digested in the phagolysosome, the macrophages enhance the expression of genes involved in the assembly and release of lipoproteins and the production of storage peptides. Macrophages thus convert the raw cellular matter into an easily transportable and exploitable form of lipoproteins and storage peptides, to be subsequently used for post-metamorphic maturation. The intervention of macrophage production of lipoproteins by silencing *apolpp* expression in these cells leads to delayed ovary development and reduced fecundity. Thus, the macrophages promote the transfer of energy between the larval and adult life stage.

Our data indicate that under certain conditions *Drosophila* macrophages can acquire metabolically nutritive roles and generate suitable nutrients from digested cellular remnants to support other tissues in the body. Although this metabolic role might be rather unexpected for macrophages, this function may originate from the nutritive phagocytosis that is currently hypothesized to precede the macrophage protective role in immune response (Hartenstein and Martinez, 2019). The process of phagocytosis and processing of engulfed material is highly conserved within the animal clade. Even the free-living unicellular ancestors of all animals performed phagocytosis to obtain nutrients from engulfed bacteria and foreign eukaryotic cells (Desjardins et al., 2005). A similar form of nutritive phagocytosis is common also in multicellular animals, in which professional nutritive phagocytes process endocytosed material and provide it in a suitable form to other cells in the body (Mills, 2020). Macrophages as professional phagocytes play a central role in maintaining tissue homeostasis by clearing damaged, apoptotic and senescent cells (Lavin et al., 2015). In this process, which is essential for the health of tissues and organs, tens of billions of cells are removed and replaced by new ones every day in the human body (Doran et al., 2020). Based on our data, it is reasonable to assume that the nutritive value of these cells and the building blocks they contain are not merely wasted. However, whether macrophages play an analogous role during metamorphosis of amphibians, embryonal morphogenesis, as well as daily cellular turnover, remains to be discovered.

The mechanism of macrophage metabolic polarization during metamorphosis may be complex and has not yet been fully elucidated. One trigger that induces the adoption of a transient adipocyte-like polarization of *Drosophila* macrophages may be their mere exposure to the histolyzing cells along with the excessive amount of leaking lipids, ribosomes and other cellular fragments (Elliott et al., 2017). Presumably, these lipids originate mainly from the dying larval adipocytes and possibly from larval muscles, which have been shown to be also infiltrated by macrophages during metamorphosis (Regan et al., 2013; Ghosh et al., 2020). In parallel, the macrophage function may also be affected by hormonal signaling. Ecdysone, the most important regulator of metamorphosis in arthropods, has been shown to be a potent regulator of macrophages during *Drosophila* metamorphosis. It enhances macrophage motility and triggers the expression of genes involved in the enzymatic remodeling of the extracellular matrix, neutralization of toxic compounds and efferocytosis (Regan et al., 2013).

The adoption of macrophage adipocyte-like metabolic polarization may have also an alternative explanation. At the onset of metamorphosis, the adipocytes retain storage peptides from the circulation and sequester the endoplasmic reticulum and RNA into RNP granules (Tysell and Butterworth, 1978). These transient organelles resemble the stress granules, the formation of which in response to stress conditions has been extensively studied in many mammalian and insect cell lines. The formation of RNP granules protects the presynthesized mRNA molecules from their degradation, resulting in stalled translation under adverse conditions (Ivanov et al., 2019; Kipper et al., 2022). After overcoming the period of stress, mRNA translation can be promptly restored (Riggs et al., 2020; Campos-Melo et al., 2021). As the RNP granules can leak from larval adipocytes in *Drosophila* and may be frequently found disentangled in the macrophage cytosol, we hypothesize that the mRNA bound in RNP granules may serve as a template for translation in macrophages, which may thus acquire the adipocyte-like features. This strategy may be particularly efficient in the case of larval adipocytes, which produce mRNA in multiple copies from polytene chromosomes. Although there is no clear evidence supporting this hypothesis, this phenomenon deserves more attention in future research.

Over the past decade, the role of macrophages in insect metamorphosis has been considered negligible (Nelliot et al., 2006). Recently, however, it has been demonstrated that macrophages show a striking level of resistance to the tools used in these initial attempts of

Development (2024) 151, dev202492. doi:10.1242/dev.202492

their depletion and that macrophage function is essential for successful progress of metamorphosis (Stephenson et al., 2022). It is evident that macrophages interact closely with the larval adipocytes and engulf them via efferocytosis (Ghosh et al., 2020). The phenotypic profile of macrophages during post-metamorphic development is of particular interest when compared with two independent single-cell RNA-seq analyses of *Drosophila* larval hemocytes. In these publications, the authors identified subpopulations of plasmatocytes, which upregulate the expression of lipophorins and storage peptides, denoted as adipohemocytes or secretory plasmatocytes (Tattikota et al., 2020; Cattenoz et al., 2020).

Infiltration of adipose tissue by macrophages is a hallmark of obesity, diabetes and metabolic syndrome (Boutens and Stienstra, 2016; Mirzoyan et al, 2023). Nevertheless, recent observations have revealed that adipose tissue is also infiltrated in other situations of metabolic stress such as starvation, dyslipidemia, and bacterial or viral infection (Surmi and Hasty, 2008; Kosteli et al., 2010; Silva et al., 2019). These observations indicate that the adipose tissue-associated macrophages may play a hitherto undiscovered role in the regulation of metabolism and the clearance of exhausted and moribund adipocytes. Although *D. melanogaster* represents a frequently used model organism for the study of human diseases including diabetes, metabolic syndrome or cachexia, the model has suffered from the under-investigated interaction between macrophages and adipocytes (Graham and Pick, 2017; Álvarez-Rendón et al., 2018; Chatterjee and Perrimon, 2021; Mirzoyan et al, 2023). Here, we describe an adaptive physiological process, during which macrophages display features observed otherwise in mammalian macrophages under pathophysiological conditions such as metabolic syndrome, obesity and atherosclerosis (Hariri et al., 2000). We believe that our discoveries may open novel avenues for the study of obesity and obesity-related diseases in the *Drosophila* model.

MATERIALS AND METHODS

Drosophila melanogaster strains and culture

The flies were raised on a diet containing cornmeal (80 g/l), sucrose (50 g/l), yeast (40 g/l), agar (10 g/l) and 10%-methylparaben (16.7 ml/l) and maintained in a humidity-controlled environment with a natural 12 h light/12 h dark cycle at 25°C. The larvae were developed in vials with plenty of food and particular care was taken not to have too many individuals in one vial to avoid possible adverse effects that could be attributed to metabolic or other stress. Flies were categorized according to their morphological features, and no obvious differences in developmental time or pupal mortality were observed unless explicitly stated in the manuscript. The flies of the following genotypes were used in the crosses resulting in the genotypes analyzed: *apolpp*$^{RNAi\ KK}$, Bloomington Drosophila Stock Center (BDSC), 28946; *apolpp*$^{RNAi\ GD}$, Vienna Drosophila Resource Center (VDRC), V6878; CrqGal4>2xeGFP, provided by Marc C. Dionne (Imperial College London, UK); Hml-dsRed, provided by Marc C. Dionne; Lpp-GFP, VDRC, v318255; Lsp2Gal4, BDSC, 6357; TRiP^{control}, BDSC, 35786; EcR^{DN}, BDSC, 6872; BirA, BDSC, 93424; UAS-Grim, provided by John Nambu (Stanford University, CA, USA); UAS-Rpr; UAS-Hid, provided by John Nambu; Hml$^{e9\text{-}P2a}$ Gal4, provided by Alf Herzig (Max Planck Institute for Infection Biology, Berlin, Germany); Atg8a-mCherry, provided by Gabor Juhasz (Max Planck Institute for Infection Biology, Berlin, Germany).

Phenotypic analyses

Pupariation rate analyses

Sixty larvae of a given genotype were placed in individual vials. Their developmental status was checked at regular daily intervals and the number of pupated individuals was counted. The experiments were carried out in an incubator with controlled light and dark regime and controlled temperature and humidity. These data were recorded by a data logger and checked regularly.

Egg laying analysis

Twenty-five freshly emerged virgins of a given genotype were placed in a vial containing ten males of the control genotype. Each day, flies were transferred to a fresh vial and the number of eggs laid was counted for the subsequent 3 days.

Eclosion rate analysis

The eclosion rate was assessed by counting the number of flies that emerged from 75 larvae placed in a vial containing standard fly food. Experiments were conducted in an incubator with controlled light and dark regime and controlled temperature and humidity.

Counting of adipocytes

To determine the number of larval adipocytes on the fly abdomen, flies were anesthetized and adipocytes were washed from the ruptured abdomen in a drop of PBS on a microscope slide. Analysis was performed on an inverted microscope. Larval adipocytes were identified by characteristic morphological features in the bright field.

Tissue dissections and isolations

Isolation of macrophages

Macrophages were isolated from flies based on the expression of endogenous GFP protein in these cells. *Crq>Gal4 UAS-eGFP* male flies were used for isolation of macrophages using fluorescence-activated cell sorting (FACS). The flies were anesthetized with CO_2, washed in PBS and homogenized in 600 ml of ice-cold PBS using a pestle. The homogenate was sieved through a nylon cell strainer (40 µm). This strainer was then additionally washed with 200 µl of ice-cold PBS, which was then added to the homogenate. The samples were centrifuged (3 min, 4°C, 1509 ***g***) and the supernatant was washed with ice-cold PBS after each centrifugation (three times). Before sorting, samples were transferred to FACS polystyrene tubes using a disposable bacterial filter (50 µm, Sysmex) and macrophages were sorted into 100 µl of PBS using an S3^{TM} Cell Sorter (Bio-Rad). Isolated cells were verified by fluorescence microscopy and differential interference contrast for their morphology and viability. Different numbers of isolated macrophages were used in different subsequent analyses. To this end, different numbers of flies were used for their isolation, specifically 90 flies were used to isolate 20,000 macrophages for qPCR analysis; ∼160 flies were used to isolate 50,000 macrophages for metabolic analysis; ∼300 flies were used to isolate 100,000 and 200,000 macrophages for lipidomic and transcriptomic analyses, respectively.

Isolation of hemolymph

For hemolymph isolation, 25 flies for each sample were anesthetized on ice and punctured in the abdomen and thorax. Flies were then transferred to Eppendorf tubes with a silica membrane, covered with glass beads, and spun in a centrifuge (10 min, 4°C, 9700 ***g***). The hemolymph was collected at the bottom of a collection tube containing 50 µl of ice-cold PBS to prevent hemolymph clotting and melanization. The supernatant was transferred into a fresh Eppendorf tube to avoid possible contaminants from circulating plasmatocytes.

Isolation of the fat body and ovaries

To isolate the larval fat body residues and ovaries from the abdomen, subjects were dissected in ice-cold PBS. Individuals destined for dissection were attached with tiny entomological pins to a Sylgard polymer-coated dish. The abdomen was opened with spring scissors in five sections and the abdomen was spread and secured at the corners with additional pins. For subsequent metabolic and confocal analyses, ovaries were carefully dissected with tweezers by pulling them out of the body by the oviduct. The individual free-floating adipocytes were collected by pipette with a wide bore 1 ml pipette tip. These samples do not contain any adult adipocytes as adult adipose tissue is formed by sheets of polygonal cells, which are attached to the cuticle.

Development (2024) 151, dev202492. doi:10.1242/dev.202492

Gene expression analysis

The macrophages were isolated using a cell sorter as described above. Macrophages were subsequently transferred to TRIzol Reagent (Invitrogen) and homogenized using a DEPC-treated pestle. RNA was extracted by TRIzol Reagent (Invitrogen) according to the manufacturer's protocol. Superscript III Reverse Transcriptase (Invitrogen) primed by oligo(dT)20 primer was used for reverse transcription. Relative expression rates for particular genes were quantified on a 384CFX 1000 Touch Real-Time Cycler (Bio-Rad) using the TP 2x SYBR Master Mix (Top-Bio) in three technical replicates according to the following protocol: initial denaturation, 3 min at 95°C; amplification, 15 s at 94°C, 20 s at 56°C, 25 s at 72°C for 40 cycles. Melting curve analysis was performed at 65-85°C/step 0.5°C. The qPCR data were analyzed using double delta Ct analysis, and the expression of *apolpp* was normalized to the expression of Ribosomal protein 49 (Rp49; RpL32; FBgn0002626) in the corresponding sample. The relative values (fold change) to control are shown in the graphs. Primers used in this work were: *apolpp* – forward TTGGAATCCTAGCTTCTGTGCT (CG11064, FBgn0087002), reverse AGTCATAGTAGTTGCCGGGTAT (CG11064, FBgn0087002); *Rp49* – forward AAGCTGTCGCACAAATGGCG (CG7939, FBgn0002626), reverse GCACGTTGTGCACCAGGAAC (CG7939, FBgn0002626).

Measurement of cholesterol and cholesteryl-ester in macrophages

To measure metabolite concentration in macrophages, the samples were split for the isolation of metabolites and proteins that were used for sample normalization if not stated otherwise. Samples were homogenized in 200 µl of PBS and centrifuged (3 min, 4°C, 7800 ***g***) to discard insoluble debris. For the analysis of metabolites in macrophages, the sample was obtained from 90 individuals. Samples for analysis of lipids were processed by an adapted protocol originally developed by Bligh and Dyer for the isolation of lipid fraction from biological samples (Bligh and Dyer, 1959). A Bicinchoninic Acid Assay (BCA) Kit (Sigma-Aldrich) was used for protein quantification according to the supplier's protocol and the absorbance was measured at 595 nm. Cholesterol and cholesteryl esters were measured on isolated lipid fraction using the Cholesterol/Cholesteryl Ester Quantitation Kit (Sigma-Aldrich) according to the supplier's protocol. Samples for metabolite concentration were collected from four independent experiments.

Preparation of paraffin sagittal sections and Mallory trichrome staining

The individuals were fixed in 4% paraformaldehyde (PFA) in PBS for 2 h. For pupal stages, the layers of the puparium were removed before fixation. All the analyzed individuals were punctured by a tungsten needle before fixation. After prefixation in PFA, specimens were post-fixed in Bouin-Hollande solution [BHS; picric acid (0.9%), formaldehyde (9%), acetic acid (5%), 10% $HgCl_2$ and distilled water]. Samples were fixed in BHS for 24 h. Dehydrated samples were subsequently embedded in paraffin, sectioned at a thickness of 10 µm on a rotation microtome (Leica RM2165) and stained by Mallory trichrome staining. Sagittal sections were analyzed using an inverted fluorescent microscope (Olympus Axioplan BX63).

Efficiency of macrophage ablation

For determining the efficiency of macrophage ablation, two *Hml*$^{e9\text{-}P2A\text{-}GAL4>TubGal80^{TS}}$; *UAS Grim* flies and two controls (*Hml*$^{e9\text{-}P2A\text{-}GAL4>TubGal80^{TS}}$) were used per biological replicate. The abdomen of freshly emerged flies was opened in a drop of PBS on a microscope slide and the adipocytes were flushed out. The macrophages were left to attach to the slide for 40 min. Thereafter, the macrophages were stained by anti-NimC1 antibody (1:100, kindly provided by István Andó, Biological Research Centre, Szeged, Hungary; Kurucz et al., 2007). The images were taken on an Olympus FluoView 3000 confocal microscope (Olympus).

HPF freezing and TEM

For the transmission electron microscopy (TEM) analysis, flies were fixed by the high-pressure freezing (HPF)/freeze substitution (FS) method. The fly abdomens were frozen in the presence of 20% bovine serum albumin using a Leica EM PACT2 high-pressure freezer. FS (FSLeica EM ASF2) was carried in 2% OsO_4 diluted in 100% acetone at −90°C for 96 h. Then specimens were warmed up at a rate of 5°C h^{-1}, left at −20°for 24 h and at 4°C for another 24 h. At room temperature, specimens were rinsed three times in 100% acetone and incubated in a graded series of SPI-pon resin (SPI) solutions (25%, 50%, 75%) diluted in acetone, for 1 h at each step. Tissues were incubated in pure resin overnight, embedded in fresh resin, and polymerized at 60°C for 48 h. Ultrathin sections (70 nm) were cut using an ultramicrotome Leica UCT (Leica Microsystems), counterstained with uranyl acetate for 30 min and lead citrate for 20 min. Samples were examined by a JEOL TEM 1010 operated at 80 kV. The TEM images were false-colorized in Adobe Photoshop software.

X-ray computed tomography

For the micro-computed tomography analysis, the flies were anesthetized using CO_2, dipped in 70% ethanol to remove the hydrophobic layer, and submerged into the BHS for at least 3 days. Subsequently, the samples were thoroughly washed in 1× PBS and transferred to Lugol solution (Sigma-Aldrich, L6146-1L) for at least 4 days for tissue contrast. The flies were then washed in mineral oil (Sigma-Aldrich, 330779-1L) and scanned in a 10 µm pipette tip using the SkyScan 1272 (Bruker) at source voltage 40 kV, source current 200uA, image pixel size 1.4 µm, and rotation step 0.100°. The reconstruction was carried out in NRecon and 3D visualization was achieved in CTVox Micro-CT Volume Rendering Software (Bruker). The segmentation, computation of the volume of ovaries and computation of the relative percentage of ovary volume to the volume of the fly's body were conducted in the Avizo software (Thermo Fisher Scientific) using the Volume Fraction module.

Staining of lipids

Flies were dissected in ice-cold PBS and fixed with 4% PFA in PBS (Polysciences). After 20 min, the tissues were washed and stained for neutral lipids using NileRed or Bodipy. Lipid staining was accompanied by the staining of nuclei and cytoskeleton, which allowed us to infer the morphology of the tissue and to quantify adequately the amount of lipids in the cells. The tissues were then washed and mounted in an Aqua Polymount (Polysciences). Tissues were imaged using an Olympus FluoView 3000 confocal microscope. The content of lipids in macrophages, ovaries and larval adipose tissue was analyzed using Fiji software. Samples were collected in four independent experiments and representative images are shown.

Immunostaining

Flies were dissected in ice-cold PBS and fixed with 4% PFA in PBS (Polysciences) for 20 min. After three washes in PBS-Tween (0.1%), nonspecific binding was blocked by 10% normal goat serum in PBS for 1 h at room temperature (RT). Tissues were then incubated with primary antibodies (mouse anti-NimC1 antibody P1a+b, 1:100) at 4°C overnight. After washing the unbound primary antibody (three times for 10 min in PBS-Tween), the secondary antibody was applied at a dilution of 1:250 for 2 h at RT [goat anti-mouse IgG (H+L) Alexa 555 or goat anti-mouse IgG (H+L) Cy2]. Nuclei were stained with DAPI. Tissues were mounted with Aqua Polymount (Polysciences). Tissues were imaged using an Olympus FluoView 3000 confocal microscope and images were reconstructed using Fiji software.

Lipidomic analysis

Fat bodies from six flies and 100,000 isolated macrophages were obtained for each analyzed group. Tissue lipid fraction was extracted by 500 µl of cold chloroform:methanol solution (v/v; 2:1). The samples were then homogenized by a Tissue Lyser II (Qiagen) at 50 Hz, −18°C for 5 min and kept further in an ultrasonic bath (0°C, 5 min). Further, the mixture was centrifuged at 10,000 rpm (12,320 ***g***) at 4°C for 10 min followed by the removal of the supernatant. The extraction step was repeated under the same conditions. The lower layer of pooled supernatant was evaporated to dryness under a gentle stream of argon. The dry total lipid extract was re-dissolved in 50 µl of chloroform:methanol solution (v/v; 2:1) and directly measured

Development (2024) 151, dev202492. doi:10.1242/dev.202492

using a standard method: briefly, high-performance liquid chromatography (Accela 600 pump, Accela AS autosampler) combined with mass spectrometry LTQ-XL (all Thermo Fisher Scientific) were used. The chromatographic conditions were as follows: injection volume 5 µl; column Gemini 3 µM C18 HPLC column (150×2 mm ID, Phenomenex) at 35°C; the mobile phase (A) 5 mM ammonium acetate in methanol with ammonia (0.025%), (B) water and (C) isopropanol: methanol (8:2); gradient change of A:B:C as follows: 92:8:0 (0 min), 97:3:0 (7 min), 100:0:0 (12 min), 93:0:7 (19 min), 90:0:10 (20-29 min), 40:0:60 (40-45 min), 100:0:0 (48 min) and 92:8:0 (50-65 min) with flow rate 200 µl/min. The mass spectrometry condition was: positive (3 kV) and negative (−2.5 kV) ion detection mode; capillary temperature 200°C. Eluted ions were detected with full scan mode at 200-1000 Da with the collisionally induced MS2 fragmentation (NCE 35). Data were acquired and processed by means of XCalibur 4.0 software (Thermo Fisher Scientific). The corrected areas under individual analytical peaks were expressed in percentages assuming that the total area of all detected is 100%. Lipidomics data were subsequently analyzed in the online platform LipidSuite (https://suite.lipidr.org/). Data were inputted by the K-Nearest Neighbors method (KNN), and normalization was performed using the PQN algorithm. Subsequently, data were explored by principal component analysis and orthogonal partial least squares-discriminant analysis methods. Differential analysis of lipidomic data was carried out by univariate analysis and visualized in volcano plots.

Proteomic analysis

The hemolymph samples were subjected to in-solution digestion before mass spectrometry (MS) analysis. Proteins were reduced with 10 mM 1,4-dithiothreitol (DTT) at 56°C for 45 min and alkylated with 55 mM iodoacetamide at RT in the dark for 20 min. The alkylation was quenched with 50 mM DTT. Trypsin (Sigma-Aldrich) was used for proteolytic fragmentation at a ratio of 50:1 (protein:trypsin) overnight at 37°C. The digestion was terminated by the addition of formic acid to a final concentration of 2.5% and peptides were purified using Stage tip solid-phase C18 discs.

The obtained peptides were dissolved in 30 µl of 3% acetonitrile/0.1% formic acid. The peptide analysis was carried out on an UltiMate 3000 RSLCnano system (Thermo Fisher Scientific) on line coupled to mass spectrometer timsTOF Pro (Bruker Daltonics). The peptide solution of 2 µl was injected onto an Acclaim™ PepMap™ 100 C18 trapping column (300 µm i.d., 5 mm length, particle size 5 µm, pore size 100 Å; Thermo Fisher Scientific) at a 2.5 µl/min flow rate of 2% acetonitrile/0.1% formic acid for 2 min. The peptides were eluted from the trapping column onto an Acclaim™ PepMap™ 100 C18 analytical column (75 µm i.d., 150 mm length, particle size 2 µm, pore size 100 Å; Thermo Fisher Scientific) and separated by a 48 min long linear gradient of 5-35% acetonitrile/0.1% formic acid at a constant flow rate of 0.3 µl/min. The column oven temperature was set at 35°C. Data were acquired in PASEF scan mode with positive polarity. Electrospray ionization was performed using a CaptiveSpray (Bruker Daltonics) with capillary voltage at 1500 V, dry gas at 3 l/min and dry temperature at 180°C. Ions were accumulated for 100 ms and ten PASEF MS/MS scans were acquired per topN acquisition cycle. An ion mobility range (1/K0) was set at 0.6-1.6 Vs/cm^2. Mass spectra were collected over an m/z range of 100-1700. A polygon filtering was applied to exclude the low m/z of singly charged ions. The target intensity was set at 20,000 to repeatedly select precursors for PASEF MS/MS repetitions. The precursors that reached the target intensity were then excluded for 0.4 min. Collision energies were changed from 20 to 59 eV in five steps of equal width between 0.6 and 1.6 Vs/cm^2 of 1/K0 values.

Raw MS data were processed in MaxQuant software (version 1.6.14) with an integrated Andromeda search engine. Database of *D. melanogaster* available in Uniprot (08. 11. 2022) supplemented with the contaminant database included in the MaxQuant software was used to identify proteins. The default parameters for the TIMS-DDA search type and Bruker TIMS instrument were applied. Trypsin/P was set as an enzyme allowing up to two missed cleavages in specific digestion mode; the carbamidomethylation of cysteine was used as fixed modification; N-terminal protein acetylation and methionine oxidation were applied as variable modifications; the minimum and maximum peptide length was set to 8 and 25 amino acids, respectively. Precursor ion tolerance was set at 20 and 10 ppm in the first and the main peptide search, respectively; the mass tolerance for MS/MS fragment ions was set at 40 ppm. Peptide Spectrum Match (PSM) and protein identifications were filtered using a target-decoy approach at a false discovery rate of 1%. Label-free quantification of proteins was carried out using the algorithm integrated into MaxQuant.

Protein tables obtained from MaxQuant were analyzed using Perseus software (version 1.6.14.0). The data were filtered to eliminate hits to the reverse database, contaminants and proteins were only identified with modified peptides. Proteins identified by only one peptide along with a score lower than 40 were excluded from further analysis.

Incorporation of ^{13}C free fatty acids

For assaying ^{13}C-FFA distribution during post-metamorphic development, the larvae were reared on fly food containing 50 µl ^{13}C Fatty Acid Mix (Cambridge Isotope Laboratories), 5 mg/ml in chloroform per each vial, for 5 h. Analysis of ^{13}C content in the fat body and the rest of the body indicates that this approach led to ∼80% of labeled carbons accumulating in the larval fat body. Freshly emerged individuals were transferred to unlabeled food and remnants of larval fat body, hemolymph and ovaries were analyzed for ^{13}C content 48 h after eclosion. Lipid fraction from the samples was isolated through an adapted Bligh and Dyer procedure and free fatty acids were deliberated from complexes by a lipase from *Aspergillus niger*. Homogenized and filtered chloroform extracts (100 µl) were put in glass inserts in 2 ml chromatographic vials and their ^{13}C enrichment was analyzed compound-specific. Then 1 µl was injected in a split/splitless injector of a gas chromatograph (GC; Trace 1310, Thermo Fisher Scientific), injector at 250°C. The injection was splitless for 1.5 min, then split with flow 100 ml/min for 1 min, and 5 ml/min (gas saver) for the rest of the analysis. Semipolar capillary column Zebron, ZB-FFAP (Phenomenex; 30 m×0.25 mm×0.25 µm film thickness) with a flow rate of 1.5 ml/min of helium was used as a carrier. The temperature program was: 50°C during injection and for the next 2 min, then 50-200°C with a slope of 30°C/min, 200-235°C with a slope of 3°C/min, and hold at 235°C for the remaining 32 min (total run time ∼51 min). Eluting compounds were oxidized to CO_2 via IsoLink II interphase (Thermo Fisher Scientific) at 1000°C and introduced to continuous-flow isotope ratio MS (Delta V Advantage, Thermo Fisher Scientific). Compounds were identified using retention times of fatty acid standards. ^{13}C sample abundance was expressed in At-% ^{13}C and '^{13}C excess' calculated as: ^{13}C excess=A^{13}Cs−A^{13}Cn, where A^{13}Cs is the absolute ^{13}C abundance of labeled samples and A^{13}Cn is the absolute ^{13}C abundance of natural lipids.

Transcriptomic analysis

For transcriptomic analysis, macrophages isolated from wandering larvae, freshly emerged individuals and 10-day-old flies were used. The details of the isolation procedure are as described above. We used 200,000 macrophages for the isolation of RNA by TRIzol (Ambion). Sequencing libraries were prepared using siTOOLs riboPOOL *D. melanogaster* RNA kit (EastPort) followed by subtraction of ribosomal fraction by NEBNext Ultra II Directional RNA kit (Illumina). The quality of prepared RNA libraries was assayed by Bioanalyzer and all samples reached an RIN score over the threshold of 7. Sequencing analysis was performed by using the NovaSeq instrument (Illumina). Raw sequencing data were processed using the standard bioinformatics workflow for trimming barcodes and adapters. Trimmed reads were aligned to the reference *D. melanogaster* genome BDGP6.95 (Ensembl release). Trimming, mapping and analysis of quality were performed in CLC Genomic Workbench 21.0.5 software via the standard workflow for RNA-seq and differential gene expression analysis. A subsequent search of transcriptomic data for enhanced and silenced pathways and biological processes was carried out using TCC, and iDep94 platforms combined with String and FlyMine databases.

Phagocytic activity

Flies with induced tools for macrophage depletion were injected with 50 nl of pHrodo™ Red *S. aureus* (Thermo Fisher Scientific) to assay their phagocytic capability. After 45 min, the abdomens of analyzed flies were

Development (2024) 151, dev202492. doi:10.1242/dev.202492

dissected in PBS and then fixed for 20 min with 4% PFA. Aqua Polymount (Polysciences) was used to mount the sample. Macrophages were imaged using an Olympus FluoView 3000 confocal microscope and red dots depicting phagocytic events were counted manually per cell.

Tissue-specific tracing of proteins (BirA)

Circulating proteins were analyzed for their site of origin in freshly emerged flies and flies 10 days after emergence. For this purpose, flies carrying promiscuous biotin ligase either under macrophage-specific or fat body-specific promotor were generated (*CrqGal4>UAS Bir-A*; *FB-Gal4>UAS Bir-A*). These flies were held over their development on diet with an enhanced content of biotin prepared according to Droujinine et al. (2021). Briefly, biotin diluted in ethanol was added to the standard *Drosophila* diet before completely cooling to a final concentration of 50 µM. Hemolymph from an analyzed individual was isolated as stated above. The hemolymph samples were spun by centrifugation (8900 ***g***, 10 min at room temperature) to avoid any cellular contaminants. The biotinylated protein fraction was subtracted by magnetic separation by using streptavidin-coated magnetic particles (Sigma-Aldrich) according to the manufacturer's instructions. Along with subtraction, samples of hemolymph from control genotypes and samples processed without magnetic isolation were processed and analyzed for the identification of naturally highly biotinylated circulating proteins.

Statistics

Box plots, heat maps and donut graphs were generated in GraphPad Prism9 software. Ordinary one-way ANOVA followed by Dunnett's multiple comparisons test was used to compare the results with the corresponding control group. A two-tailed unpaired *t*-test was used for pair reciprocal comparison of datasets. Bar plots display mean and standard deviation. The statistical significance of the test is depicted by $*P<0.05$, $**P<0.001$, $***P<0.0001$. Normality and homogeneity of variations were tested by the Anderson-Darling test, D'Agostino Pearsons' test and Shapiro-Wilk test. Data showing significant deviances from normal distribution were normalized by Log2-transformation. For complex differential analysis of omics data, we processed the data through an online platform for transcriptomic data analysis (TCC, based on the R-packages *edgeR*, *DESeq*, *baySeq* and *NBPSeq*, and iDep95, based on the R-packages *limma*, *DESeq2*, *GSEA*, *PAGE*, *GACE*, *RactomePA*, *Kallisto* and *Galaxy*), followed by subsequent analysis of assigned biological processes in Kegg pathways (www.genome.jp/kegg/pathway.html) and Flymine databases (https://www.flymine.org/flymine). An online platform for lipidomic data analysis (LipidSuite, based on the R-package *lipidr*) was employed for differential comparison of obtained lipidomic datasets.

Acknowledgements

We thank Lucie Hrádková for laboratory services and support. We thank the Laboratory of Microscopy and Histology and the Electron Microscopy Laboratory of the Biological Centre of the Czech Academy of Sciences for assistance in the preparation of histological samples. We thank Mark C. Dionne, Gabor Juhasz, Alf Herzig and John Nambu for providing the fly lines. Other fly populations were obtained from the BDSC and the VDRC. We also thank Petra Berkova and Petr Simek for lipidomics services, and the Department of Medical Biology (USB) for allowing the use of the S3eBioRad sorter. We thank the developers of Fiji (an open-source platform for bioimaging analysis; doi:10.1038/nmeth.2019), LipidSuite (a suitable platform for lipidomic analysis), TCC (an online platform for transcriptomic data processing) and iDep94 (an alternative online platform for transcriptomic data analysis). Graphical summaries used in project conceptualization and data presentation were created with BioRender.com.

Competing interests

The authors declare no competing or financial interests.

Author contributions

Conceptualization: G.K., A.B.; Methodology: G.K., A.D., H.S., F.D., J.K., M.M., A.B.; Software: G.K., A.B.; Validation: G.K., H.S., A.B.; Formal analysis: G.K., H.S., F.D., J.K., M.M., A.B.; Investigation: G.K., A.D., H.S., F.D., J.K., M.M., A.B.; Resources: G.K., A.B.; Data curation: G.K., A.D., H.S., F.D., J.K., M.M., A.B.; Writing - original draft: G.K., A.B.; Writing - review & editing: G.K., A.B.; Visualization: G.K., A.D., H.S., A.B.; Supervision: G.K., A.B.; Project administration: G.K., A.B.; Funding acquisition: G.K., A.B.

Funding

The authors gratefully acknowledge financial support from the Grantová Agentura České Republiky for A.B. (20-14030S and 23-06133S). G.K. was supported by the Jihočeská Univerzita v Českých Budějovicích Grant Agency (050/2019/P).

Data availability

The datasets produced in this study are available in the following databases: RNA-seq data have been deposited in GEO under accession number GSE237617. Lipidomic data are available from the Dryad Digital Repository (Bajgar, 2023): dryad.9zw3r22kw.

The people behind the papers

This article has an associated 'The people behind the papers' interview with some of the authors.

Peer review history

The peer review history is available online at https://journals.biologists.com/dev/lookup/doi/10.1242/dev.202492.reviewer-comments.pdf

References

Aguila, J. R., Suszko, J., Gibbs, A. G. and Hoshizaki, D. K. (2007). The role of larval fat cells in adult Drosophila melanogaster. *J. Exp. Biol.* **210**, 956-963. doi:10.1242/jeb.001586

Álvarez-Rendón, J. P., Salceda, R. and Riesgo-Escovar, J. R. (2018). Drosophila melanogaster as a model for diabetes type 2 progression. *BioMed Res. Int* **2018**, 1-16. doi:10.1155/2018/1417528

Aouadi, M., Vangala, P., Yawe, J. C., Tencerova, M., Nicoloro, S. M., Cohen, J. L., Shen, Y. and Czech, M. P. (2014). Lipid storage by adipose tissue macrophages regulates systemic glucose tolerance. *Am. J. Physiol. Endocrinol. Metab.* **307**, E374-E383. doi:10.1152/ajpendo.00187.2014

Bajgar, A. (2023). Lipidomic data of macrophages isolated from adult fruit flies (Drosophila melanogaster) 24 hours post-infection [Dataset]. *Dryad Digital Repository*. doi:10.5061/dryad.9zw3r22kw

Barth, J. M. I., Szabad, J., Hafen, E. and Köhler, K. (2011). Autophagy in Drosophila ovaries is induced by starvation and is required for oogenesis. *Cell Death Differ.* **18**, 915-924. doi:10.1038/cdd.2010.157

Bligh, E. G. and Dyer, W. J. A. (1959). Rapid method of total lipid extraction and purification. *J. Biochem. Physiol.* **37**, 911-917.

Bond, N. D., Nelliot, A., Bernardo, M. K., Ayerh, M. A., Gorski, K. A., Hoshizaki, D. K. and Woodard, C. T. (2011). ßFTZ-F1 and Matrix metalloproteinase 2 are required for fat-body remodeling in Drosophila. *Dev. Biol.* **360**, 286-296. doi:10.1016/j.ydbio.2011.09.015

Boutens, L. and Stienstra, R. (2016). Adipose tissue macrophages: going off track during obesity. *Diabetologia* **59**, 879-894. doi:10.1007/s00125-016-3904-9

Butterworth, F. M., Emerson, L. and Rasch, E. M. (1988). Maturation and degeneration of the fat body in the Drosophila larva and pupa as revealed by morphometric analysis. *Tissue Cell* **20**, 255-268. doi:10.1016/0040-8166(88)90047-X

Campos-Melo, D., Hawley, Z. C. E., Droppelmann, C. A. and Strong, M. J. (2021). The integral role of RNA in stress granule formation and function. *Front. Cell Dev. Biol.* **9**, 621779. doi:10.3389/fcell.2021.621779

Cattenoz, P. B., Sakr, R., Pavlidaki, A., Delaporte, C., Riba, A., Molina, N., Hariharan, N., Mukherjee, T. and Giangrande, A. (2020). Temporal specificity and heterogeneity of Drosophila immune cells. *EMBO J.* **39**, e104486. doi:10.15252/embj.2020104486

Chatterjee, N. and Perrimon, N. (2021). What fuels the fly: Energy metabolism in Drosophila and its application to the study of obesity and diabetes. *Sci. Adv.* **7**, eabg4336. doi:10.1126/sciadv.abg4336

Cho, B., Yoon, S.-H., Lee, D., Koranteng, F., Tattikota, S. G., Cha, N., Shin, M., Do, H., Hu, Y., Oh, S. Y. et al. (2020). Single-cell transcriptome maps of myeloid blood cell lineages in Drosophila. *Nat. Commun.* **11**, 4483. doi:10.1038/s41467-020-18135-y

Dahik, V. D., Frisdal, E. and Le Goff, W. (2020). Rewiring of lipid metabolism in adipose tissue macrophages in obesity: impact on insulin resistance and Type 2 diabetes. *Int. J. Mol. Sci.* **21**, 5505. doi:10.3390/ijms21155505

Desjardins, M., Houde, M. and Gagnon, E. (2005). Phagocytosis: the convoluted way from nutrition to adaptive immunity. *Immunol. Rev.* **207**, 158-165. doi:10.1111/j.0105-2896.2005.00319.x

Doran, A. C., Yurdagul, A. and Tabas, I. (2020). Efferocytosis in health and disease. *Nat. Rev. Immunol.* **20**, 254-267. doi:10.1038/s41577-019-0240-6

Droujinine, I. A., Meyer, A. S., Wang, D., Udeshi, N. D., Hu, Y., Rocco, D., McMahon, J. A., Yang, R., Guo, J. J., Mu, L. et al. (2021). Proteomics of protein trafficking by in vivo tissue-specific labeling. *Nat. Commun.* **12**, 2382. doi:10.1038/s41467-021-22599-x

Elliott, M. R., Koster, K. M. and Murphy, P. S. (2017). Efferocytosis signaling in the regulation of macrophage inflammatory responses. *J. Immunol.* **198**, 1387-1394. doi:10.4049/jimmunol.1601520

Elliott, M. R. and Ravichandran, K. S. (2016). The dynamics of apoptotic cell clearance. *Dev. Cell* **38**, 147-160. doi:10.1016/j.devcel.2016.06.029

Franz, A., Wood, W. and Martin, P. (2018). Fat body cells are motile and actively migrate to wounds to drive repair and prevent infection. *Dev. Cell* **44**, 460-470.e3. doi:10.1016/j.devcel.2018.01.026

Ghosh, S., Ghosh, S. and Mandal, L. (2020). Drosophila metamorphosis involves hemocyte mediated macroendocytosis and efferocytosis. *Int. J. Dev. Biol.* **64**, 319-329. doi:10.1387/ijdb.190215lm

Graham, P. and Pick, L. (2017). 'Drosophila as a model for diabetes and diseases of insulin resistance. *Curr. Top. Dev. Biol.* **121**, 397-419. doi:10.1016/bs.ctdb.2016.07.011

Hariri, M., Millane, G., Guimond, M.-P., Guay, G., Dennis, J. W. and Botstein, D. (2000). Biogenesis of multilamellar bodies via autophagy. *Mol. Biol. Cell.* **11**, 255-268. doi:10.1091/mbc.11.1.255

Hartenstein, V. and Martinez, P. (2019). Phagocytosis in cellular defense and nutrition: a food-centered approach to the evolution of macrophages. *Cell Tissue Res.* **377**, 527-547. doi:10.1007/s00441-019-03096-6

Hochreiter-Hufford, A. and Ravichandran, K. S. (2013). Clearing the dead: apoptotic cell sensing, recognition, engulfment, and digestion. *Cold Spring Harbor Perspect. Biol.* **5**, a008748-a008748. doi:10.1101/cshperspect.a008748

Ivanov, P., Kedersha, N. and Anderson, P. (2019). Stress granules and processing bodies in translational control. *Cold Spring Harbor Perspect. Biol.* **11**, a032813. doi:10.1101/cshperspect.a032813

Juarez-Carreño, S., Vallejo, D. M., Carranza-Valencia, J., Palomino-Schätzlein, M., Ramon-Cañellas, P., Santoro, R., de Hartog, E., Ferres-Marco, D., Romero, A., Peterson, H. P. et al. (2021). Body-fat sensor triggers ribosome maturation in the steroidogenic gland to initiate sexual maturation in Drosophila. *Cell Rep.* **37**, 109830. doi:10.1016/j.celrep.2021.109830

Kiger, J. A., Natzle, J. E. and Green, M. M. (2001). Hemocytes are essential for wing maturation in Drosophila melanogaster. *Proc. Natl Acad. Sci. USA* **98**, 10190-10195. doi:10.1073/pnas.181338998

Kipper, K., Mansour, A. and Pulk, A. (2022). Neuronal RNA granules are ribosome complexes stalled at the pre-translocation state. *J. Mol. Biol.* **434**, 167801. doi:10.1016/j.jmb.2022.167801

Kosteli, A., Sugaru, E., Haemmerle, G., Martin, J. F., Lei, J., Zechner, R. and Ferrante, A. W. (2010). Weight loss and lipolysis promote a dynamic immune response in murine adipose tissue. *J. Clin. Investig.* **120**, 3466-3479. doi:10.1172/JCI42845

Kurucz, E., Márkus, R., Zsámboki, J., Folkl-Medzihradszky, K., Darula, Z., Vilmos, P., Udvardy, A., Krausz, I., Lukacsovich, T., Gateff, E. et al. (2007). Nimrod, a putative phagocytosis receptor with EGF repeats in Drosophila plasmatocytes. *Curr. Biol.* **17**, 649-654. doi:10.1016/j.cub.2007.02.041

Lavin, Y., Mortha, A., Rahman, A. and Merad, M. (2015). Regulation of macrophage development and function in peripheral tissues. *Nat. Rev. Immunol.* **15**, 731-744. doi:10.1038/nri3920

Leader, D. P., Krause, S. A., Pandit, A., Davies, S. A. and Dow, J. A. T. (2018). FlyAtlas 2: a new version of the Drosophila melanogaster expression atlas with RNA-Seq, miRNA-Seq and sex-specific data. *Nucleic Acids Res.* **46**, D809-D815. doi:10.1093/nar/gkx976

Lei, Y., Huang, Y., Yang, K., Cao, X., Song, Y., Martín-Blanco, E. and Pastor-Pareja, J. C. (2023). FGF signaling promotes spreading of fat body precursors necessary for adult adipogenesis in Drosophila. *PLoS Biol.* **21**, e3002050. doi:10.1371/journal.pbio.3002050

Li, Y., Yun, K. and Mu, R. (2020). A review on the biology and properties of adipose tissue macrophages involved in adipose tissue physiological and pathophysiological processes. *Lipids Health Dis.* **19**, 164. doi:10.1186/s12944-020-01342-3

Locke, M. and Collins, J. V. (1965). The structure and formation of protein granules in the fat body of an insect. *J. Cell Biol.* **26**, 857-884. doi:10.1083/jcb.26.3.857

Mezu-Ndubuisi, O. J. and Maheshwari, A. (2021). Role of macrophages in fetal development and perinatal disorders. *Pediatr. Res.* **90**, 513-523. doi:10.1038/s41390-020-01209-4

Mills, D. B. (2020). The origin of phagocytosis in Earth history. *Interface Focus* **10**, 20200019. doi:10.1098/rsfs.2020.0019

Mirzoyan, Z., Valenza, A., Zola, S., Bonfanti, C., Arnaboldi, L., Ferrari, N., Pollard, J., Lupi, V., Cassinelli, M., Frattaroli, M. et al. (2023). A Drosophila model targets Eiger/TNFα to alleviate obesity-related insulin resistance and macrophage infiltration. *Dis. Model Mech.* **16**, dmm050388. doi:10.1242/dmm.050388

Murray, P. J. and Wynn, T. A. (2011). Protective and pathogenic functions of macrophage subsets. *Nat. Rev. Immunol.* **11**, 723-737. doi:10.1038/nri3073

Nelliot, A., Bond, N. and Hoshizaki, D. K. (2006). 'Fat-body remodeling in Drosophila melanogaster'. *Genesis* **44**, 396-400. doi:10.1002/dvg.20229

Palm, W., Sampaio, J. L., Brankatschk, M., Carvalho, M., Mahmoud, A., Shevchenko, A. and Eaton, S. (2012). Lipoproteins in Drosophila melanogaster—Assembly, function, and influence on tissue lipid composition. *PLoS Genet.* **8**, e1002828. doi:10.1371/journal.pgen.1002828

Phan, V. H., Herr, D. R., Panton, D., Fyrst, H., Saba, J. D. and Harris, G. L. (2007). Disruption of sphingolipid metabolism elicits apoptosis-associated reproductive defects in Drosophila. *Dev. Biol.* **309**, 329-341. doi:10.1016/j.ydbio.2007.07.021

Poças, G. M., Crosbie, A. E. and Mirth, C. K. (2022). When does diet matter? The roles of larval and adult nutrition in regulating adult size traits in Drosophila melanogaster. *J. Insect Physiol.* **139**, 104051. doi:10.1016/j.jinsphys.2020.104051

Regan, J. C., Brandão, A. S., Leitão, A. B., Mantas Dias, A. R., Sucena, E., Jacinto, A. and Zaidman-Rémy, A. (2013). Steroid hormone signaling is essential to regulate innate immune cells and fight bacterial infection in Drosophila. *PLoS Pathog.* **9**, e1003720. doi:10.1371/journal.ppat.1003720

Rehman, N. and Varghese, J. (2021). Larval nutrition influences adult fat stores and starvation resistance in Drosophila. *PLoS ONE* **16**, e0247175. doi:10.1371/journal.pone.0247175

Riggs, C. L., Kedersha, N., Ivanov, P. and Anderson, P. (2020). Mammalian stress granules and P bodies at a glance. *J. Cell Sci.* **133**, jcs242487. doi:10.1242/jcs.242487

Rode, S., Ohm, H., Anhäuser, L., Wagner, M., Rosing, M., Deng, X., Sin, O., Leidel, S. A., Storkebaum, E., Rentmeister, A. et al. (2018). Differential requirement for translation initiation factor pathways during ecdysone-dependent neuronal remodeling in Drosophila. *Cell Rep.* **24**, 2287-2299.e4. doi:10.1016/j.celrep.2018.07.074

Schmitz, G. and Muller, G. (1991). Structure and function of lamellar bodies, lipid-protein complexes involved in storage and secretion of cellular lipids. *J. Lipid Res.* **32**, 1539-1570.

Silva, H. M., Báfica, A., Rodrigues-Luiz, G. F., Chi, J., Santos, P. d. A., Reis, B. S., Hoytema van Konijnenburg, D. P., Crane, A., Arifa, R. D. N., Martin, P. et al. (2019). Vasculature-associated fat macrophages readily adapt to inflammatory and metabolic challenges. *J. Exp. Med.* **216**, 786-806. doi:10.1084/jem.20181049

Stephenson, H. N., Streeck, R., Grüblinger, F., Goosmann, C. and Herzig, A. (2022). Hemocytes are essential for Drosophila melanogaster post-embryonic development, independent of control of the microbiota. *Development* **149**, 18. doi:10.1242/dev.200286

Storelli, G., Nam, H.-J., Simcox, J., Villanueva, C. J. and Thummel, C. S. (2019). Drosophila HNF4 directs a switch in lipid metabolism that supports the transition to adulthood. *Dev. Cell* **48**, 200-214.e6. doi:10.1016/j.devcel.2018.11.030

Surmi, B. and Hasty, A. (2008). Macrophage infiltration into adipose tissue: initiation, propagation and remodeling. *Future Lipidol.* **3**, 545-556. doi:10.2217/17460875.3.5.545

Tattikota, S. G., Cho, B., Liu, Y., Hu, Y., Barrera, V., Steinbaugh, M. J., Yoon, S.-H., Comjean, A., Li, F., Dervis, F. et al. (2020). A single-cell survey of Drosophila blood. *eLife* **9**, e54818. doi:10.7554/eLife.54818

ten Brink, H., de Roos, A. M. and Dieckmann, U. (2019). The evolutionary ecology of metamorphosis. *Am. Nat.* **193**, E116-E131. doi:10.1086/701779

Tsuyama, T., Hayashi, Y., Komai, H., Shimono, K. and Uemura, T. (2023). Dynamic de novo adipose tissue development during metamorphosis in Drosophila melanogaster. *Development* **150**, dev200815. doi:10.1242/dev.200815

Tysell, B. and Butterworth, F. M. (1978). Different rate of protein granule formation in the larval fat body of Drosophila melanogaster. *J. Insect Physiol.* **24**, 201-206. doi:10.1016/0022-1910(78)90035-5